UNIDIRECTIONAL SOLIDIFICATION OF UO_2-RO TYPE REFRACTORY OXIDES WITH EMPHASIS IN THE SYSTEM UO_2-MgO

A THESIS

Presented to

The Faculty of the Division of Graduate

Studies and Research

by

Min Chian Pao

In Partial Fulfillment

of the Requirement for the Degree

Master of Science in Ceramic Engineering

Georgia Institute of Technology

May, 1973

UNIDIRECTIONAL SOLIDIFICATION OF UO_2-RO TYPE REFRACTORY OXIDES WITH EMPHASIS IN THE SYSTEM UO_2-MgO

Approved:

Alan T. Chapman, Chairman

James F. Benzel

Joe K. Cochran

Date approved by Chairman

May 21, 1973

ACKNOWLEDGMENTS

The author is sincerely grateful to Dr. Alan T. Chapman for his willing assistance and needed guidance throughout this investigation. He is also grateful to Dr. James F. Benzel, and Dr. Jor K. Cochran, who served on the reading committee, for having time to review this work.

TABLE OF CONTENTS

LIST OF TABLES

LIST OF ILLUSTRATIONS

LIST OF ILLUSTRATIONS
(Continued)

LIST OF ILLUSTRATIONS
(Continued)

LIST OF ILLUSTRATIONS
(Continued)

SUMMARY

Eutectic structures in the system UO_2-MgO were produced using an internal zone melting technique. In this method the oxide mixtures were preheated in a molybdenum tube to 1500°C in a controlled atmosphere and then directly internally melted using high frequency (3.5 mhz) induction heating. Examination of various UO_2-MgO compositions indicated the "best" composites were formed using mixtures containing about 15-20 wt% MgO and 85-80 wt% UO_2 and this composition in the UO_2-MgO system, therefore, approximates the eutectic.

The additional oxides of CaO, SrO, BaO and Al_2O_3 were also unidirectionally solidified with UO_2 to form ordered oxide-oxide structures; however, none of these systems exhibited the well ordered geometries found in the UO_2-MgO samples. The ternary system UO_2-MgO-W was also investigated and eutectic structures of the various compositions solidified are presented.

CHAPTER I

INTRODUCTION

The purpose of this work was to investigate the eutectic structure formed in the UO_2-MgO system by controlling the direction of solidification of the melt. It has been known for some time that the paticular shape and arrangement assumed by eutectic crystal aggregates is strongly influenced by the way the melt is solidified. One method of controlled solidification which is presently receiving increased attention is unidriectional solidification. This method usually produces a structure where both phases tend to line up as fibers or platelets parallel to the solidification direction.

One particularly inviting area is the application of eutectics to the production of permanent magnets. A parallel array of magnetic fibers grown within a matrix of non-magnetic material should have excellent characteristics for this purpose. Another promising field for unidirectionally solidified eutectics is in the realm of electronics. For this application fibers of an electrical conductor are embedded in a semiconductor or insulator with high electrical resistence.

The actual attempt to grow unidirectional eutectics in the UO_2-MgO system is believed by this investigator to be unique, since it was not found in the literature that

anyone had attempted to grow specifically rods (or lamellar) in this system previously. However, it is understood that controlled solidification studies in this system are in progress in the Metals and Ceramics Division of the Oak Ridge National Laboratory*.

Other UO_2-RO (Al_2O_3, BaO, SrO and CaO) mixtures were studied to see if they were suitable for internal melting by induction heating before the UO_2-MgO system was chosen as the primary system to be investigated.

Tungsten additions to the UO_2-MgO system were also investigated.

* Personal Communication G. W. Clark Metals and Ceramic Div. ORNL

CHAPTER II

SURVEY OF THE LITERATURE

A combination of metals with a particularly low melting point is called a eutectic. This word " eutectic" came from a Greek word meaning " easily melted " . If eutectics are examined under the microscope, it can be seen that all of them consist of two or more types of crystals intimately mixed together. Experiments have shown that the microscopic structure of most eutectics can be drastically changed by controlling the manner in which the material is allowed to solidify. The individual crystals are sometimes sharply angular, sometimes rounded, sometiomes plate-like; occasionally they are curly like minute corn-flakes or bunched like tiny rose petals. Rapid cooling usually produces a microstructure very different from that observed when an alloy is cooled slowly[1]. This change in structure can also alter the magnetic , electric, optical, thermal and mechanical properties of the eutectics.

Lately, a unique technique unidirectional solidification has been discovered to control the micro-structure of a given eutectic. This technique is employed by obtaining a molten pool of a mixture of two metals and removing heat from a single direction so as to pass a

solidification front through the molten material[2-8].

There is considerable literature available on the metal-metal eutectic system[2-9], and some work has been done in the oxide-metal systems at the School of Ceramic Engineering at the Georgia Institute of Technology[10-14]. However, the unidirectional solidification of oxide-oxide systems in which the microstructure consists of one oxide phase in the form of lamellae or rods dispersed in a matrix of the other oxide is limited at present[15-18].

Due to the similarity of the solidification process between metal-metal systems and oxide-metal systems, the theories developed for the metals should apply to the oxide-oxide systems.

Influence of Impurities

Chadwick[2] states that in a eutectic alloy of pure metals A and B, the average composition of the solid has exactly the same composition as the liquid from which it freezes, although the component phases, alpha and beta, of the solid can be of widely different compositions. During solidification, the alpha phase rejects the atoms of B and the beta phase rejects the atoms of A. Under steady state growth conditions, the rate of rejection of B atoms by the alpha phase is equal to the rate of rejection of A atoms by the beta phase (see Figure 1).

When there was a third element present as an impurities in the alloy, Chadwick[2] found it leads to the

formation of a colony structure, which was the result of the fact that the growth rate of the individual lamellae at the cellular interfaces in not constant across the interface but in face decreases as a function of the distance from the center of a colony or cell. The curvature of the solid-liquid interface increases from the center of the cell toward the cell wall; and, since the lamellae grow normal to the solid-liquid interface, the lamellae curved as they got closer and closer to the wall of each cell, and at the cell wall were actually almost perpendicular to the direction of grwoth. He concluded from some further investigation that the colony structure of the eutectic alloys was due to the formation of a zone of constitutionally supercooled liquid ahead of the interface which was due to the rejection of the impurities in the growing solid . When the eutectic phases were found to have different partition coefficients for the same impurity element , say X , the lamellae structure may become unstable, and may be replaced by a rod type structure. The solute will build up ahead of the alpha and beta lamellae and will attain different steady state values ahead of each phase. The partition coefficient is defined as the ratio of the concentration of impurity in the solid to the concentration of impurity in the liquid with which the solid exists as any temperature. The partition coefficient of the alpha and beta lamellae were

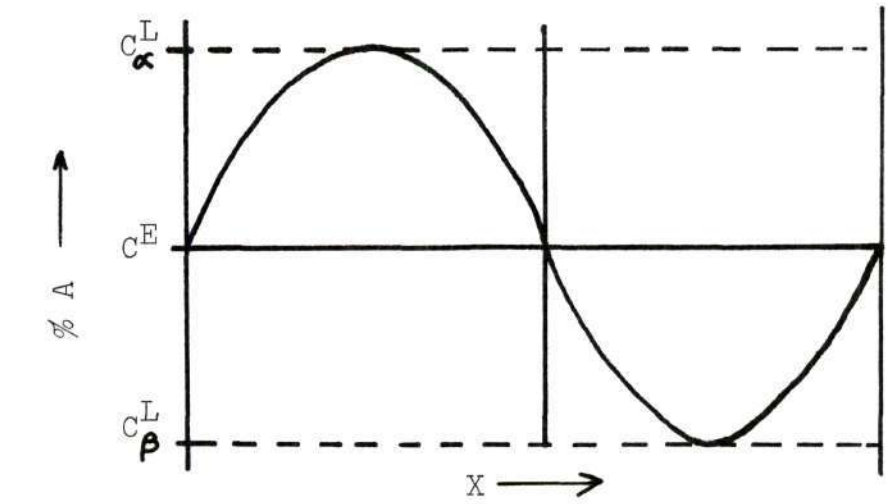

(a)

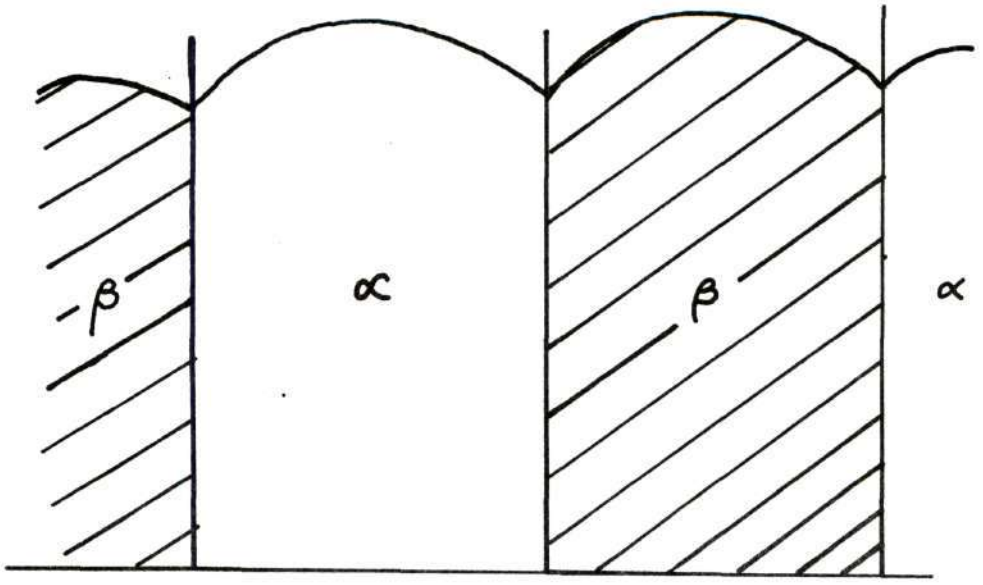

(b)

Figure 1. (a) Concentration Distribution Ahead of Eutectic Interface
(b) Shape of Eutectic Interface

C_{α}^{L} = α concentration in the liquid ahead of α phase

C_{β}^{L} = β concentration in the liquid ahead of β phase

C_{E} = Eutectic concentration
α = Lamellae phase consisted of element A
β = Lamellae phase consisted of element B

designated K_X^{α} and K_X^{β} respectively.

Assuming $K_X^{\alpha} > K_X^{\beta}$, at any steady growth rate the beta phase rejects more impurity solute, X, than the alpha phase, which means that the amount of solute at the beta lamella interface was greater than at the alpha lamella interface. Consequently, the equilibrium freezing point of the liquid in contact with the beta lamella was lower than the liquid in contact with the alpha interface. Therefore the eutectic interface was no longer isothermal, and corresponded to the difference in equilibrium temperature between two phases with the beta phase growing a finite distance behind the alpha phase, see Figure 2.

The region, just ahead of the beta lamella and between the alpha lamella, entrapes some of the solution in pockets of high solute concentration, and consequently, formed a localized zone of constitutional supercooling ahead of the beta phase. Under such conditions, the lamellar interface of the beta phase was unstable, and if any portion from beta lamella by chance protruded into the locally supercooled region, the protrusion would become stabilized. As soon as a protrusion of the beta lamella was formed, the rejection of A atoms from it would then be radial, and bridging over the beta lamella by the alpha lamella on either side of it becomes possible. The projection of the beta lamella thus became surrounded by the alpha phase, which in turn produces rods of beta. Further instabilities

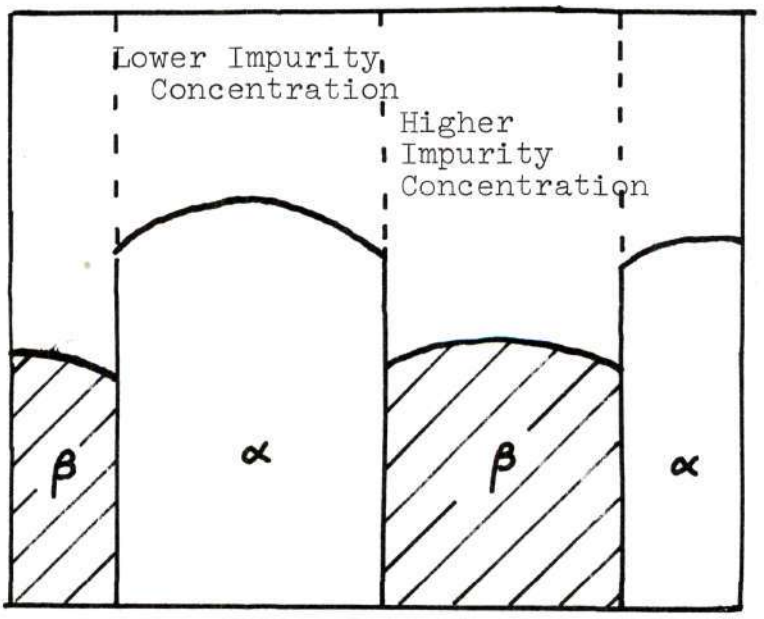

Figure 2. Profile of a Lamellar Eutectic Interface in the Presence of an Impurity Element Where $K_x^{\alpha} > K_x^{\beta}$

occurred along the length of the beta lamella and eventually the whole of the beta phase would break down into rods of beta phase lying in the growth direction, embedded in a matrix of the alpha phase. Figure 3 shows schematically the development of the rod structure form the lamellar structure.

Chadwick concluded that the addition of impurities was responsible for two growth effects within a eutectic alloy system. Such additions breaks the system down into a colony type structure, and instead of one single grain or crystal, it becomes many smaller grains or colonies. Another effect of impurities on lamellar eutectic alloys is it breaks down the lamellae type structure into a rod-like structure.

Induction Heating

The method used in heating the oxide mixtures to produce the oxide-oxide eutectic structures was induction heating. It is a clean , fast, repeatable and easily automated procedure, and provides a means for precise heating of electrically conducting objects. Induction heating occurs when the conductive materials are placed in an alternating magnetic field, produced by energizing a coil with a.c. electrical current (Figure 4) This magnetic field induces voltages in the conductive material and these voltages cause the formation of circulating currents (Eddy Currents).[19]

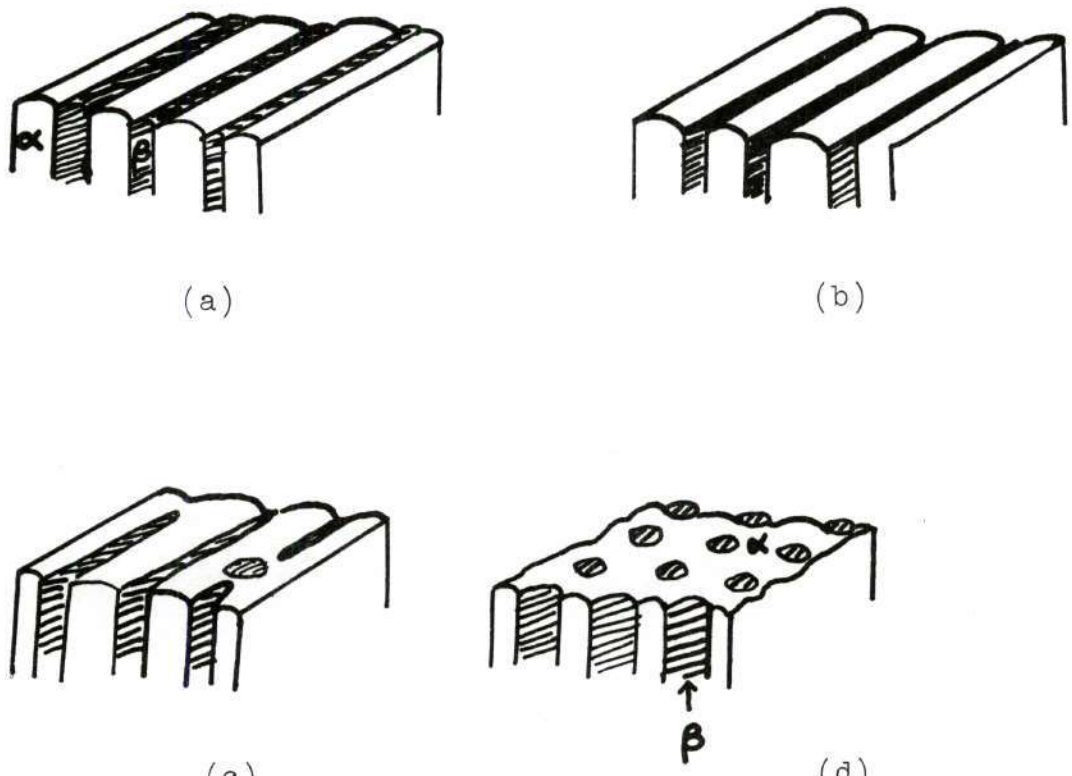

Figure 3. Schematic Drawing Illustrating the Development of a Rod-Type Structure from a Lamellar Structure.

The magnitute of these induced currents is determined by the effective magnitude of the induced voltage and by the inpedence of the material. The flow of induced current generates I^2R losses and therefore heats the workpiece.

An alternating magnetic field induces a current distribution in a conductor according to the equation:

$$\nabla^2\bar{J}=j8\pi^2\mu f\sigma x10^{-3}\bar{J} \qquad (1)$$

where $\bar{J}$ is the vector current density (amps/cm^2), j is $\sqrt{-1}$, μ is the permeability of the material, σ is the conductivity of the material (micromho/cm) and f is the frequency. Thus the current density will decrease exponentially from the surface to the interior of a conductor carrying an induced alternating current. This is known as the "skin effect" the phenomenon by which the currents flowing in the workpiece tend to be most intense at the surface, while currents at the center are near zero.

According to Leatherman and Stutz[20] the relationships between the frequency of the magnetic field and the properties of the material are not sharply critical, but they must be satisfied to the extent that the "skin effect" in the material is suitable for the desired application.

A solid cylindrical specimen will absorb power from an alternating magnetic field in relation to A* , which is the ratio of the radius to the skin depth[21], where the skin depth is defined as the depth below the surface

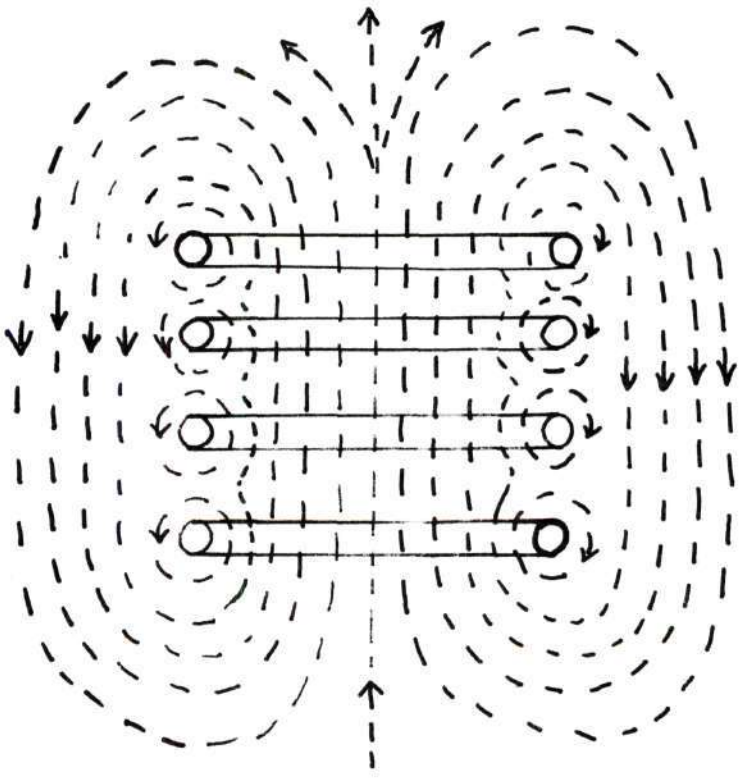

(a)

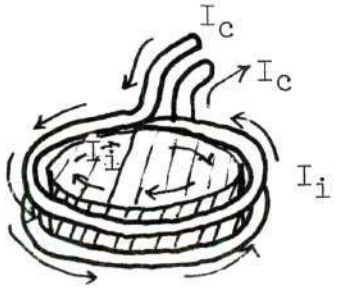

(b)

Figure 4:

(a). Electromagnetic Field Established Around the Conductor when Alternating Electric Current Flows in a Conductor.

(b). The Induced Current is Determined by the Strength of the Alternating Magnetic Field and the Spacing Between the Workpiece and the Coil , where I_c Is Coil Current and I_i Is the Induced Current in Workpiece.

of the conductor where the current density has been reduced to 1/e, or about 37 percent of the surface current density. This skin depth is related to the magnetic permeability, the frequency and the electrical conductivity by the equation:

$$\delta = (\pi \mu f \sigma)^{-1/2} \qquad (2)$$

δ = skin depth μ= magnetic permeability

f = frequency σ= electrical conductivity

A* is directly related to the ability to produce eddy current heating in a material, and is in reality a measure of the induction coil's heating efficiency. The most efficient heating occurs when A* exceeds four or five. Metals can be heated using a low frequency, but insulators requires either an increase in their conductivity or an increase in the frequency used to allow A* to reach a sufficient level for efficient heating.

The frequency used is limited , since above about 30 mhz it is very hard to contain the current on the surface of the copper work coil tubing . Arcing between the turns of the coil and to the specimen as well as increased ionization of gases further limit the frequency.

Since the frequency cannot exceed certain limits for all practical purposes, the conductivity of the material

must be raised. The method used with poor conducting materials is preheating. That is, the material is heated to a high temperature. In cases where it is disired to melt the material, the conductivity generally increases by orders of magnitude once a molted zone is initiated.

Warren[22] studied how the shape of the molted zone is affected by the conductivity and the rf frequency. Once liquid is present , some power will be dissipated in the liquid and some in the solid. If P_L is the power dissipated per unit length of the cylinder for the liquid, and P_S is the power per unit length of the solid, then the ratio P_L/P_S helps to determine the shape of the zone, since the shape depends upon a balance through-out the rod of the power generated, lost, and transferred. The shape will be normal , i.e., approximately that of a cylinder with flat caps, for common cooling conditions and $P_L/P_S \geq 1$. If, on the other hand , $P_L/P_S < 1$, more power will be generated in the solid than in the liquid, tending to melt the solid and freeze the liquid. The result is a molten zone with a liquid or a solid core, depending on A*.

The adventage of induction melting is that poor thermal conductors (i.e., the refractory oxides) retain a skin of unmelted oxide around the molten zone, and thus become their own crucible. This eliminates one source of contamination. In addition,the molten zone can be intentionally kept narrow, and can easily be moved throughout

the length of the pellet at controlled rates allowing solidification to occur in one direction.

According to Leatherman and Stutz[19], induction heating has the following advantages:

1. There is no contact required between the work load and the heat source.
2. Very high temperatures can be reached.
3. Heating is rapid.
4. Control of processing and production is simplified.
5. Higher efficiency than many other methods may be achieved.
6. Heat generation can be restricted to a surface zone of the work piece.
7. Heating may be restricted to localized areas.
8. Vacuum or controlled atmospheres may be easily used.

Unidirectional Eutectic Solidification

It has been noted before that the eutectic mixture is a composition in a two component system which has the lowest melting point of any ratio of the two components. When a liquid of the eutectic composition solidifies, the two phases co-precipitate out of the liquid. In metal alloy systems, when the eutectic alloy is unidirectionally solidifies, a structure consisting of substantially parallel alternating lamellae of each phase or long thin parallel rods of one phase embedded in a continuous matrix of the

other phase usually occurs.

According to Salkind and Lemkey [8], the only way to obtain a structure of parallel fibers and plates , or lamellae, is by unidirectional solidification. This is accomplished by removing the heat from the melt in one direction, the resulting thermal gradient producing a liquid-solid interface that is **planer.** The solidification takes place when this plane moves along the desired direction with the fibers aligned in the direction of solidification . If the interface ceases to be a plane, which happens when impurities exist and a layer of constitutionally supercooled liquid formed by impurities build-up establishes a cellular interface, then the fibers do not grow parallel, and "colonies" of fibers are often formed. A colony is an area where the fibers initiate from a central point and grow into fan shaped regions.

The spacings between the fibers or lamellae are thought to be a function of the growth rate during solidification. For a given temperature gradient and a given composition the spacing between fibers (or lamellae) increases as the growth rate decreases, since a fast growth rate would allow less time for metal atoms to diffuse through the liquid to precipitate on the nucleating tips of the fibers .

A more detailed survey of the eutectic solidification process is discussed in the following sections.

Eutectic Solidification and the Influence of Growth Rate on Lamellae Spacing

The reaction $L \rightarrow \alpha + \beta$ is called eutectic solidification, where L is liquid, α and β are two solid phases. In a eutectic , the two phases can have various morphologies. These are shown in Figure 5. The shape of the discrete phases that minimizes the amount of free energy going into the alpha-beta interface might appear to be the globular form. However , discrete globules require repeated nucleation of the second phase. It is easier (the process proceeds with less supercooling) if the second phase grows continuously as rods or lamellae. If the surface energy of the alpha-beta interface, $\gamma_{\alpha\beta}$, is independent of the orientation of the interface, rods form since these have a lower surface-to-volume ratio than do plates. However, in crystals $\gamma_{\alpha\beta}$ is rarely independent of interface orientation, so a lamellar structure is often observed, with the lamellae oriented to have a low $\gamma_{\alpha\beta}$.

The rod and lamellar eutectics occur in those cases where both phases grow with an atomically rough surface, giving an interface mobility that is high and isotropic. The liquid and solid are thus in equilibrium at each interface , so the rate of growth is determined by the rate of diffusion in the liquid.

In the case of the acicular eutectic, the matrix phase grows with an atomically rough surface, but the

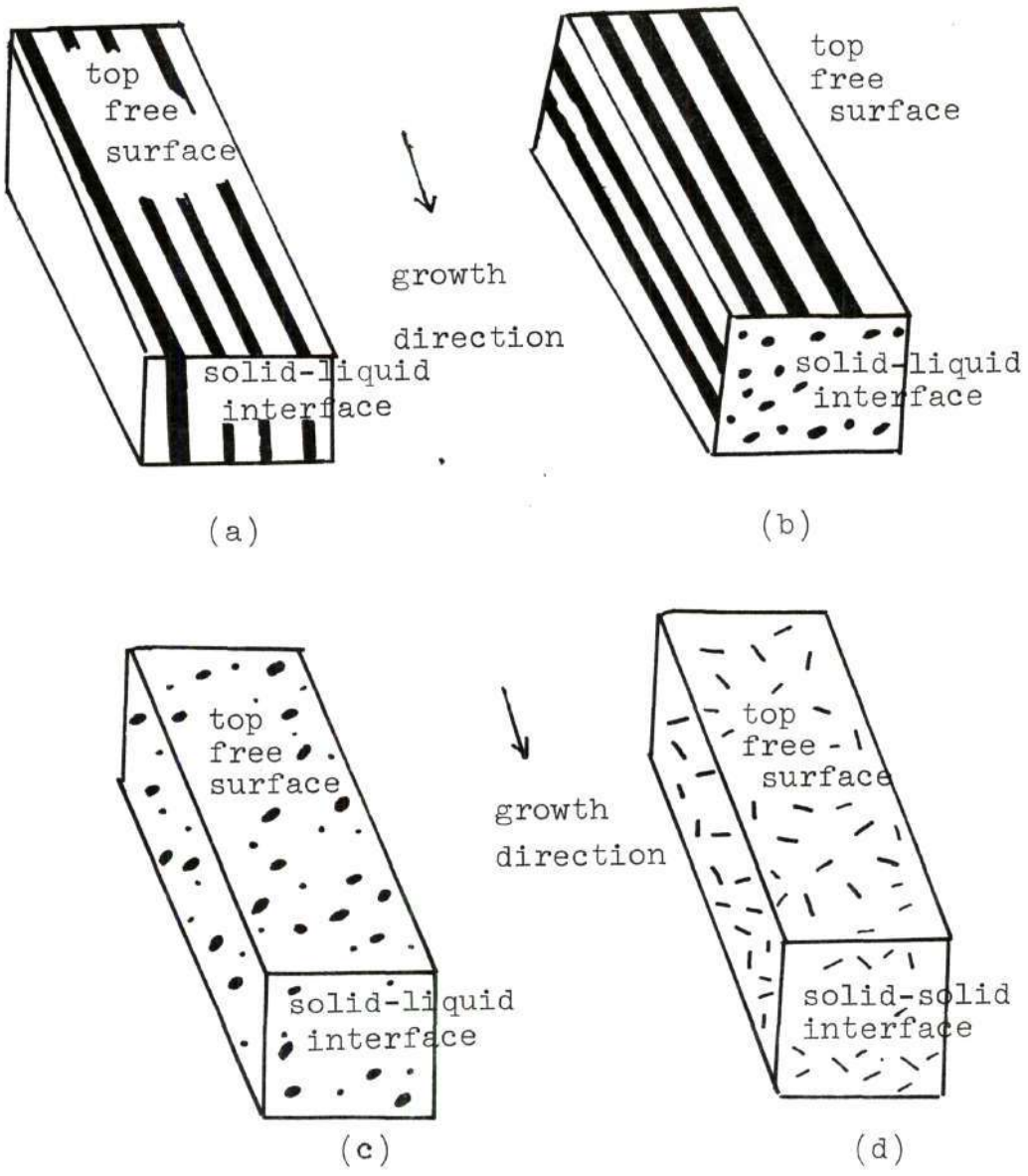

Figure 5. Schematic Illustration of Various Eutectic Structures: a. Lamellar, b. Rod-like, c. Globular, d. Acicular[23].

growth of the acicular phase is determined by the rate of incorporation of atoms into the atomically smooth crystal surface. The phase thus grows only in certain directions, rather independent of the matrix, and seems to nucleate frequently.

How fast a lamellar eutectic grows is determined by two basic considerations : the effect of the surface energy of the alpha-beta interface on the eutectic temperature, and the diffusion flow that accompanies the cooperative growth of the two phases.

The free-energy change on transforming a lamellar unit volume of liquid of eutectic composition to $\alpha + \beta$ of spacing S can be written[24]

$$\Delta G_V(S) = \Delta G_V(\infty) + \frac{\gamma_{\alpha\beta} A_{\alpha\beta}}{V} = \Delta G_V(\infty) + \frac{2\gamma_{\alpha\beta}}{S} \qquad (3)$$

where S is the center-to-center distance between lamellae and the area of α-β interface per unit volume is 2/S and $\Delta G_V(\infty)$ is the free-energy change for a spacing so large that $2\gamma_{\alpha\beta}/S$ is negligible. Figure 6 shows a free energy plot and a phase diagram that indicate the shift in eutectic temperature and solubility in the liquid resulting from the $\alpha + \beta$ as a fine lamellar eutectics. Figure 7. presents this case in terms of free-energy diagram. This diagram emphasizes the shift in the equilibrium concentration at the α-L and β-L interface

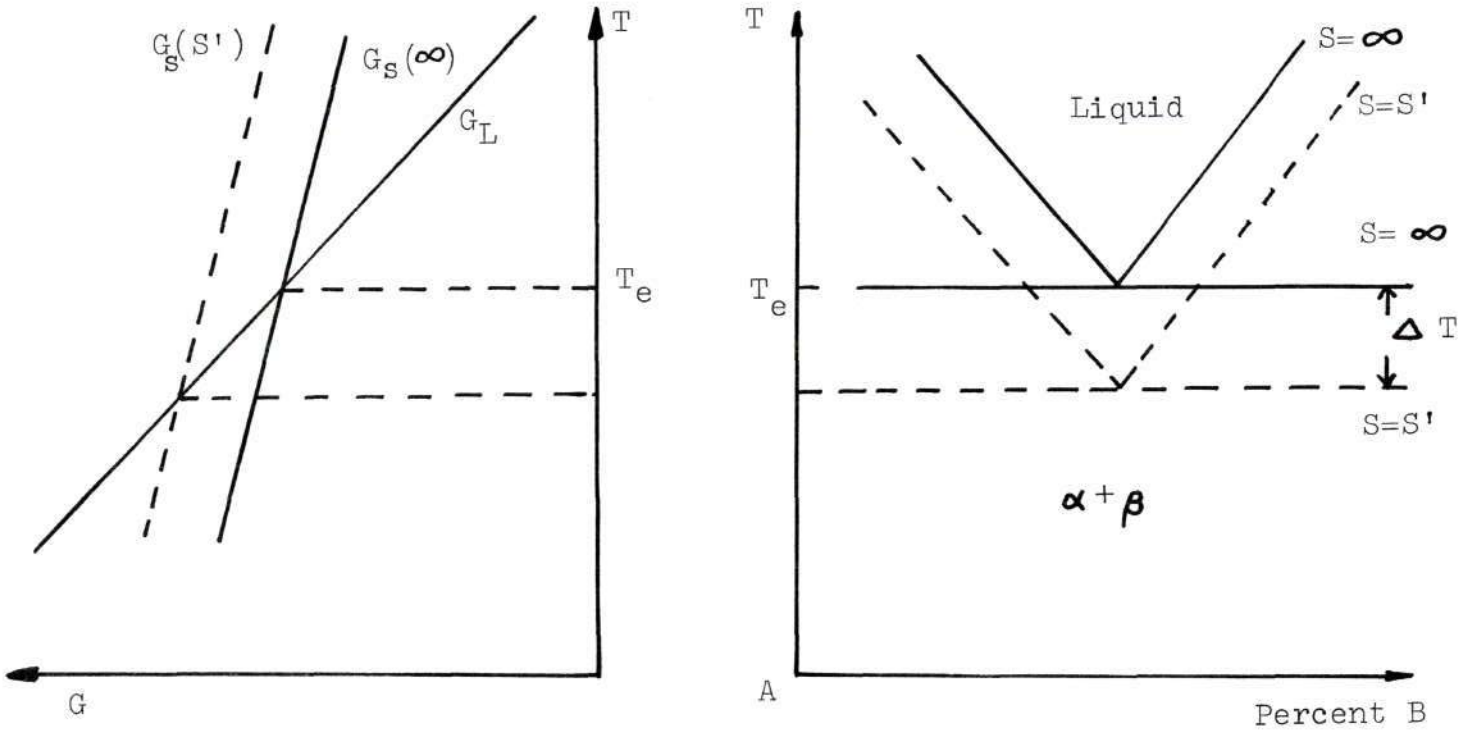

Figure 6. Free Energy vs. Temperature for a Eutectic Alloy, and Phase Diagram Showing the Depression of the Eutectic Temperature for a Lamellar Solid of Spacing S'.

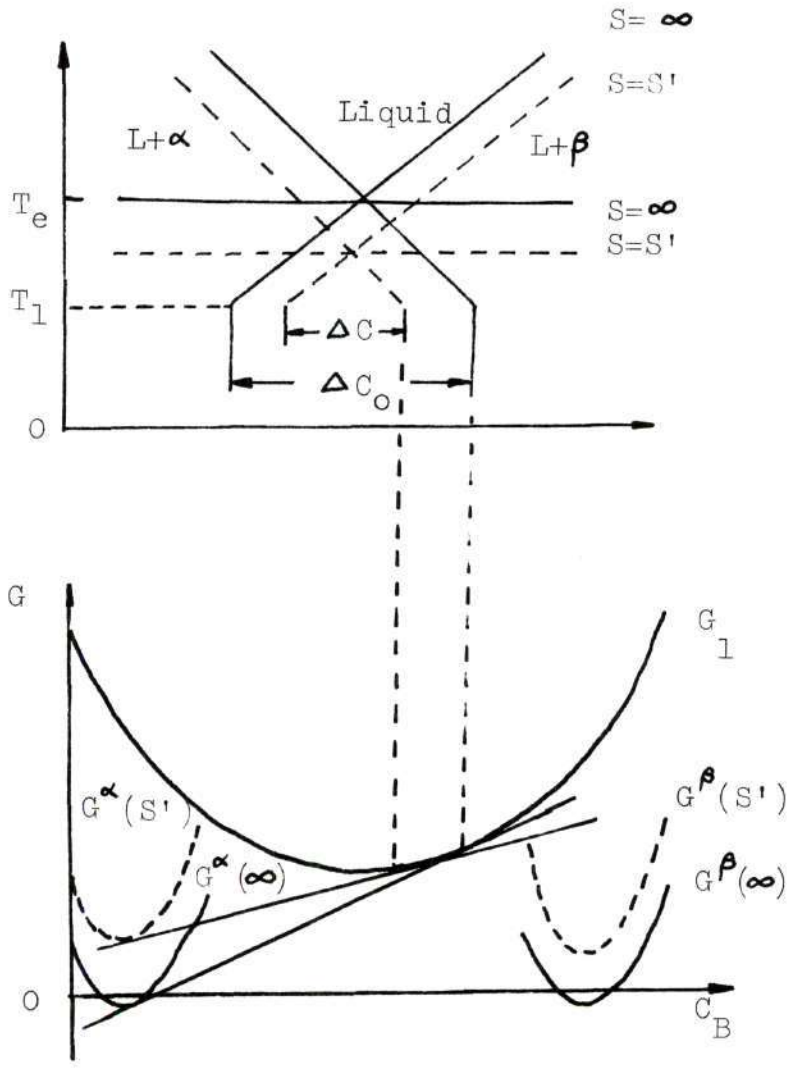

Figure 7. Free Energy Diagram for Temperature T_1 and Phase Diagram Showing the Composition of the Liquid in Equilibrium with Alpha and Beta, and How It Is Shifted When the Spacing Decreases. The Lines Labeled $S=\infty$ Are Those Normally Given on Phase Diagrams.

that results from a decrease in the lamellar spacing. It should be apparent from this that for any given undercooling ΔT below the eutectic temperature T_e, there exists a critical spacing S' such that the L, α and β are in equilibrium at this temperature $T_e - \Delta T$.

To obtain an equation for the growth velocity of the lamellar eutectic, the concentration gradients set up in frount of the α and β lamellae must be considered. Figure 8 shows these gradients as isoconcentration lines in "a", and in "b" as a section through a in front of the α and β phases. It is seen that component A piles up in front of the β and diffuses down the concentration gradient to the α phase. B diffuses in the opposite direction down a corresponding gradient. The gradient causing flow through the liquid is roughly $2\Delta C/S$, the maximum concentration drop in the liquid divided by half the spacing. As the α interface advances a distance dx in time dt, a quantity of B, $(C^{\alpha-L} - C^{L-\alpha})dx$, must move away from the interface.

The flux of B in the liquid will be toughly 2D C/S, and the quantity of solute moved in the period dt is $2D_L(C/S)dt$. If the mobility of the -L interface is high, the alpha will grow at a rate determined by this flux so

$$(C^{\alpha-L} - C^{L-\alpha})\, dx \approx 2D_L\, (\Delta C/S)\, dt \qquad (4)$$

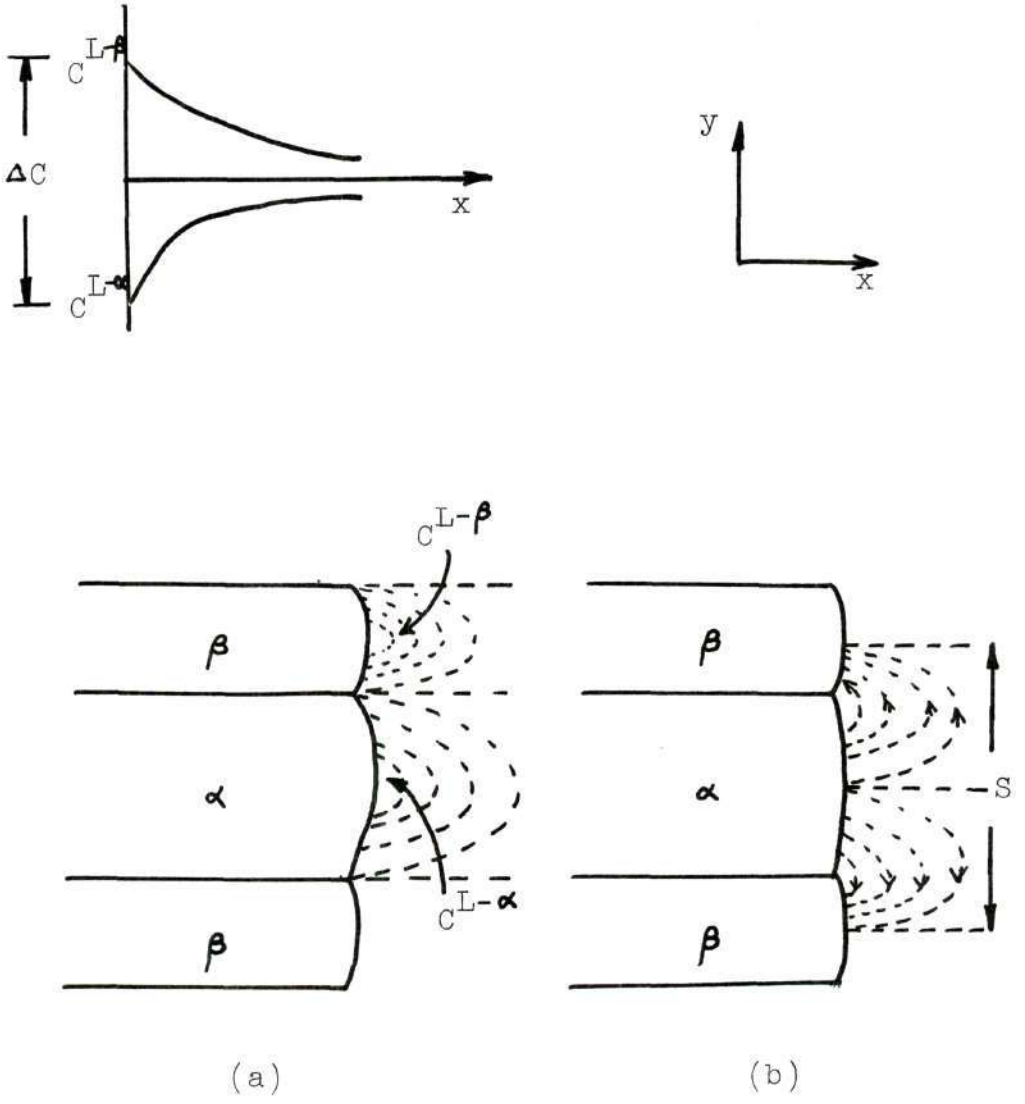

Figure 8. (a) Concentration Profiles for Component A in Liquid in Front of Growing Lamellar Eutectic Shown as Isoconcentration Lines in the x-y Plane, and Above, as C(x) in Front of Each Lamella.
(b) Arrows Show the Direction of Diffusion of A Through the Liquid in Front of the Advancing Interface.

thus

$$\frac{dx}{dt} = V_{\alpha} = \frac{D_L \Delta C}{\eta (C^{\alpha - L} - C^{L - \alpha})\, S} \qquad (5)$$

where D_L is the coefficient of diffusion of liquid, η is a constant of proportionality which is the order of unity. Both phases move at the same velocity and the equation for V_{β} will be similar, differing only in the constant η and the concentration difference in the denominator.

A first look at equation (5) might lead one to feel that spacing and the growth velocity vary inversely with one another. This is true for large S but as S approaches the critical spacing S' for the temperature of the liquid, ΔC goes to zero. Thus ΔC must be described by an equation of the form

$$\Delta C = \Delta C_o \left(1 - \frac{S'}{S} \right) \qquad (6)$$

C_o is shown in Figure 7, and is obtained by extrapolating the $S = \infty$ lines to the temperature of the interface.

Equation (5) and (6) combine to give

$$V = \frac{D_L \Delta C_o}{\eta (C^{\alpha - L} - C^{L - \alpha})\, S} \left(1 - \frac{S'}{S} \right) \qquad (7)$$

Assuming that the spacing observed in a unidirectionally solidified eutectic is that spacing which maximizes V, namely, $S = 2S'$:

$$V_m = \frac{D_L \Delta C_o}{\eta (C^{\alpha - L} - C^{L - \alpha})\, 4S'} \qquad (8)$$

At S=S', $\Delta G_V(S')$ in Eq. (3) is zero by definition. Thus

$$S' = - \frac{2 \gamma_{\alpha\beta}}{\Delta G_V (\infty)} \qquad (9)$$

But $\Delta G_V (\infty)$ is proportional to the undercooling of the liquid at the interface ΔT, so

$$S' \propto (\Delta T)^{-1} \qquad (10)$$

It is difficult to establish the temperature at the interface, and thus ΔT. However, it is relatively simple to measure the velocity of growth. If we note that $\Delta C_o \propto \Delta T$, then Eqs. (8) and (10) predict that

$$(S')^2 V_m = \text{constant} \qquad (11)$$

Experiments on unidirectionally solidified eutectics have shown that Eq. (11) is obeyed for lamellar eutectics in a wide range of alloys . They also show that the two phases tend to establish a definite orientation relative to one another. This orientation would be one which minimizes the surface tension $\gamma_{\alpha\beta}$ between the two phases and thus allows S' to be smaller for the growing lamellae.

In closing, consider the ways in which the spacing in a eutectic, S, changes so as to approximate 2S'. The mechanisms involved can be divided into those operating when S deviates substantially from 2S' for the growth conditions, and those operating when S is near 2S'. If the growth rate is suddenly increased, the spacing will

be too large for the required solute diffusion. Figure 9 (b) shows the sequence that follows. Excess solute piles up in front of the wider phase. This excess solute lowers the freezing temperature locally and makes the interface in the center of the lamellae fall behind the rest of the interface. In the pockets of higher solute concentration, the solute- rich phase nucleates and the spacing is decreased. In Figure 9 (a), the spacing has been halved by nucleating a new β particle in the center of each α lamella. Greater or lesser changes could occur by the same mechanism, depending on the density of solute-rich pockets along the regions of α-liquid interface.

If the growth rate of the eutectic is suddenly decreased, the spacing is finer than needed for solute diffusion. Some α lamellae fall behind and are eliminated from the interface. Figure 9 (c) shows such a sequence. The mechanism of spacing changes shown in Figure 9 can give changes in S of a factor of two or more.

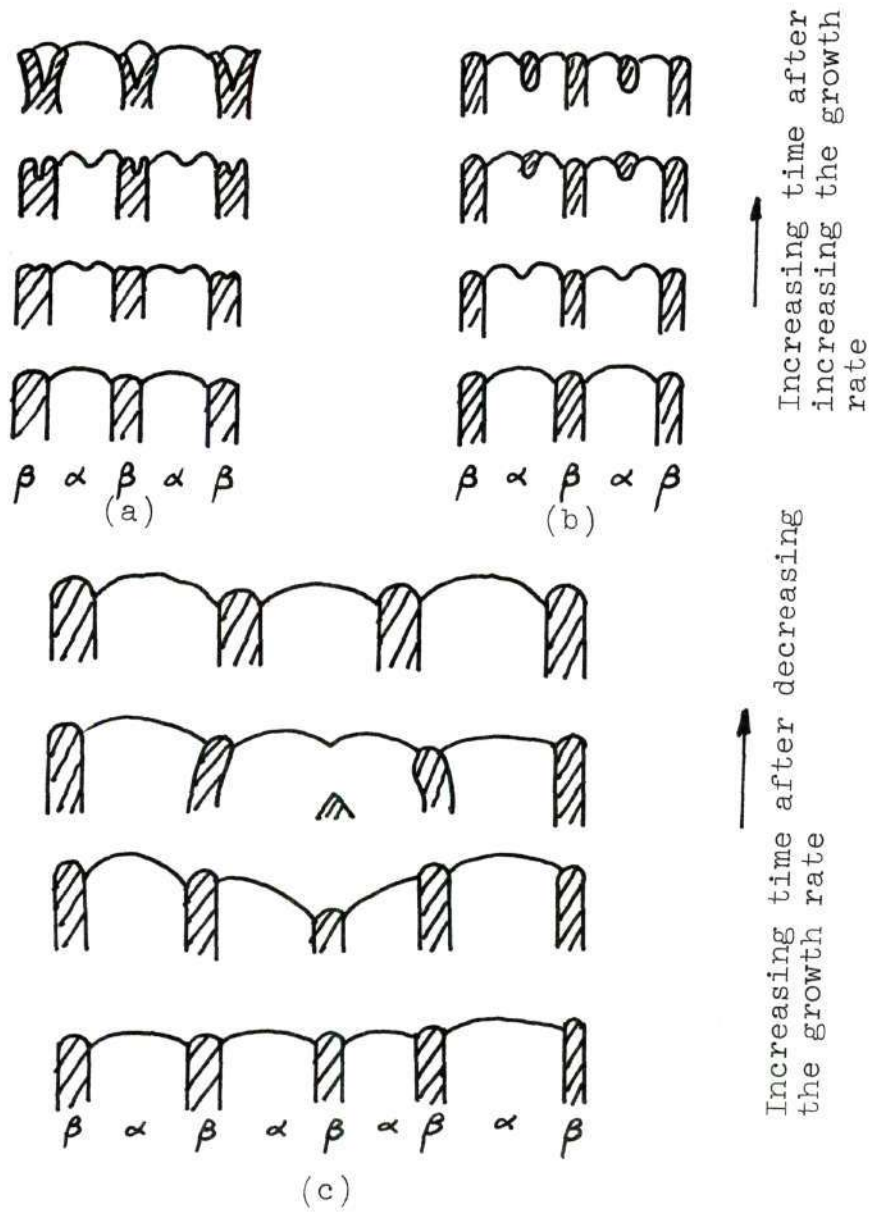

Figure 9. (a) and (b) A Series of Sketches Depicting the Changes in Interface Shape Leading to an Increase in Spacing Following a Sudden Increase in Growth Rate. Note That Only (b) Requires Nucleation of a New Phase. (c) The Decrease in Spacing Accompanying a Decrease in Growth Rate.

CHAPTER III

EQUIPMENT AND MATERIALS

Two radio frequency generators manufactured by the Lapel High Frequency Laboratories, Inc., New York were used in this investigation. One was a 10 KW output dual frequency generator capable of operating between 2.5 to 8 mhz and from 10 to 25 mhz. The other unit could be operated only at the lower frequency range.

A one inch diameter preheating tube of molybdenum was used to initially heat the sample pellet prior to direct rf heating of the samples. Provision was made for rf coupling to the preheating tube or sample pellet in a controlled atmosphsere by mounting a fused silica tube to the sample support table. The junction between the SiO_2 tube and support table was sealed with o-rings. A vaccum pump was used to evacuate the tube, the desired gases were introduced at the bottom of the tube and exited at the top, thus yielding a continuous flow of the gases by the sample area. The exhausted gas exited through a plastic tube at the top of the silica tube and were bubbled through oil to prevent back streaming into the system.

A hydraulic cylinder was used to raise and lower the sample at controlled rates. The support tube and support

assembly were mounted on a table that could be quickly lowered away from the stationary sample pellet exposing it to the rf field. Once internal melting was achieved, the pellet could be raised or lowered through the rf coils at controlled rates by the hydraulic system. The rf generator was fitted with a controller which could automatically increase or decrease the power, thus allowing slow increase in temperature during the preheating and slow cooling after the pellet had been lowered.

An overall view of the dual frequency rf generator and composite growth equipment are shown in Figure 10, and a schematic diagram of the growth facility is shown in Figure 11.

The UO_2 powder which initially had an O/U ratio of 2.14 used in the experiments was from Nuclear Material and Equipment Corporation, Appollo, Pennsylvania. A quantitative analysis certified by the same company is listed in Table 1. The MgO powder was from Fisher Scientific Company and a typical analysis of impurities is listed in Table 2. The tungsten powder was from the Fairmount Chemical Company. The sources of BaO, SrO, CaO and Al_2O_3 were unknown.

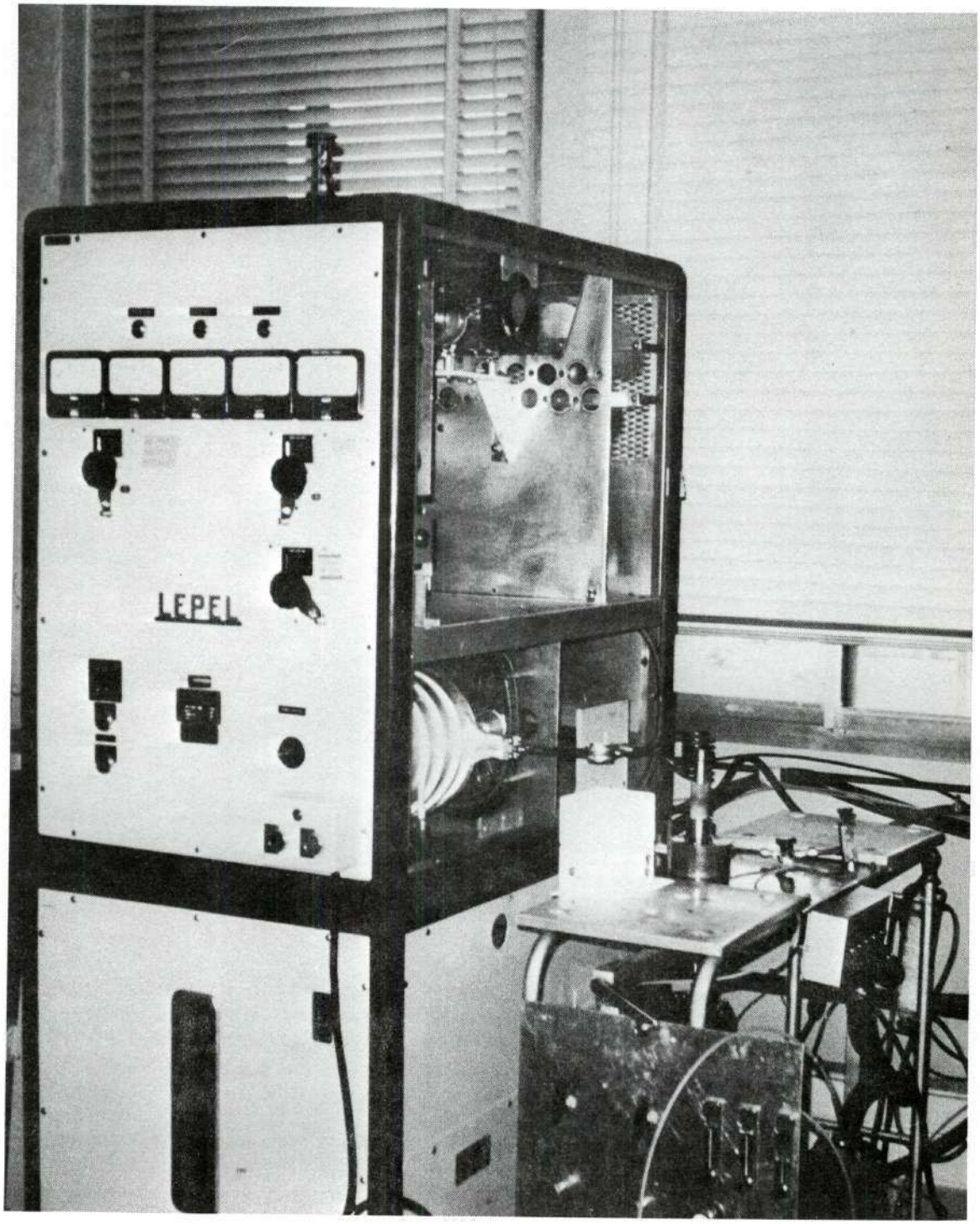

Figure 10. Overall View of the Dual Frequency rf Generator and Composite Growth Equipment.

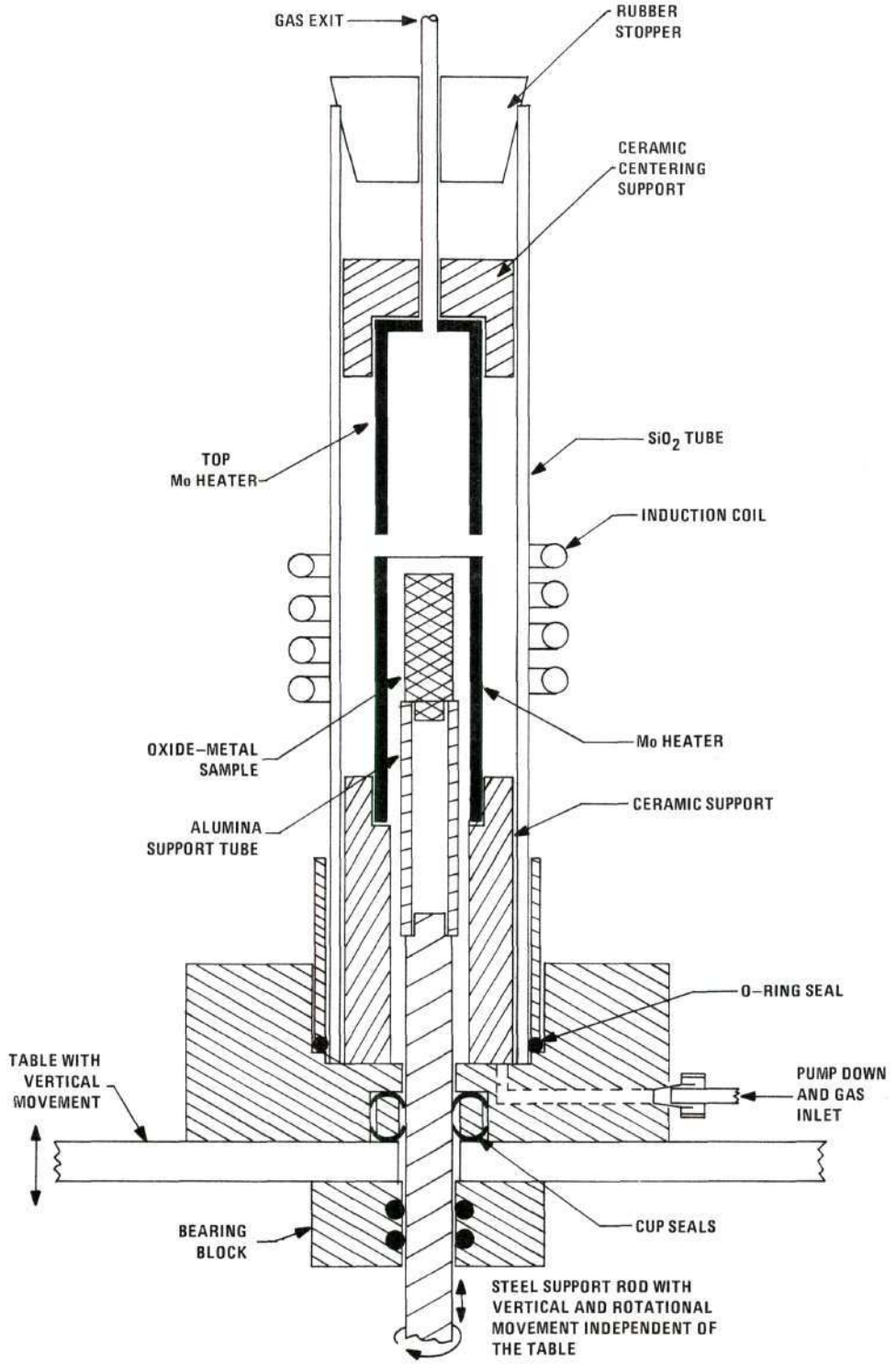

Figure 11. Schematic Diagram of the Facility for the Growth of Oxide-Oxide Composites

Table 1

Chemical Analysis of $UO_{2.14}$

ELEMENT	ANALYSIS	ELEMENT	ANALYSIS
Ag	.2	Zn	10
Ac	20	N	59
C	10	Ni	10
B	.5	Pb	2
Ca	35	Si	50
Cd	.5	Ti	10
Cl	5	V	1
Co	5	W	50
Cu	6	Dy	.02
Cr	10	Eu	.01
F	43	Gd	.02
Fe	20	Sn	.02
Mg	10	O/U (dry)	2.055
Mn	10	U%	87.87
Mo	10	H_2O	.13
Be	10	U235 %	.23
Zi	50		

(Results in PPM)

Table 2

Chemical Analysis of MgO From
Fisher Scientific Company

IMPURITIES	PERCENTAGE
Magnesium Oxide (MgO)	95.82%
Ignition Loss	1.52%
Calcium Oxide (CaO)	0.85%
Silicon Dioxide (SiO_2)	0.35%
Chloride (Cl)	0.24%
Sulfate (SO_3)	0.75%
Iron Oxide (Fe_2O_3)	0.04%
Aluminum Oxide (Al_2O_3)	0.10%
Manganese (Mn)	0.0020%
Copper (Cu)	0.0002%

CHAPTER IV

PROCEDURE

The procedure used in this experiment was divided into three sections. (1) Sample preparation; (2) Melting and solidification; and (3) Sample analysis.

Sample Preparation

The pellets used for internally melting and unidirectional solidification were small cylinders 1.9 cm in diameter and 3.75-4.38 cm in length. Previous experiments showed that this was an ideal size for induction melting with the rf generator system. The pellet was prepared by weighing the calculated amount of the required ingredients, i.e., MgO powder and UO_2 powder, then mixing those two powders in a small beaker by stirring with a spatula. The mixed powder was then poured into a 1.9cm x 10 cm die that was lubricated with a saturated solution of steric acid in acetone, and the die then tapped to settle the powder. Additional powder was then added to top off the die, and this was pressed to 1500 psi, released, and pressed again to 2500 psi. The sample was then removed from die. Sometimes the pressed pellet was crushed and remixed and repressed in order to get a denser sample.

Melting and Solidification Procedure

The sample pellet, alumina support tube, molybdenum preheater and SiO_2 tubes were all arranged as shown in Figure 11. The silica tube was evacuated to 200 militorr and then the desired gas or gas mixture was introduced, the gas flow was set at the desired rate and the rf generator was turned on. The preheating tube was heated slowly to a desired temperature by an automatic power controller. High electrical conductivity materials , such as metals, can be directly melted by induction heating but most ceramic materials do not have high enough electrical conductivity for direct heating by the alternating magnetic field. So, the preheating procedure was necessary for the oxide mixture , in order to increase their electrical conductivity so they could be internally melted by induction heating.

After preheating, power was decreased about 20 percent, and the table was lowered quickly, dropping the preheating tube away from the pellet to expose the pellet to the rf field. The power was then increased to a higher value to directly couple to the preheated pellet. The power was reduced as soon as the melt formed, since the liquid has a higher conductivity then the solid and may melt through the pellet wall if too much power was applied. It was necessary to gain experience for each oxide mixture because they required different power setting both for

rf coupling and for establishing a stable molten zone.

After coupling the sample was heated for 10 minutes in order to obtain a stable molten zone and the pellet was lowered at a controlled rate through the rf coils by the hydraulic lowering system. When the molten zone had travelled from bottom to the top of the pellet, lowering was stopped and power was reduced slowly by the automatic power controller. Thus the pellet could be cooled slowly to minimize cracking caused by rapid thermal changes.

Sample Analysis

Solidified samples were cut longitudinally parallel to the growth direction or sliced transversely with a diamond saw. The sample was then mounted in plastic for easier holding and polishing. The mounted sample was polished on and abrasive polishing wheel using decreasing grits (180, 320 and 600) of SiC abrasive papers. After the coarse polishing , a nylon cloth covered wheel was used with one micron diamond paste to polish for final microscopic examination.

The microscopic examination was done with a metallographic microscope, using both dark and light field lighting. The magnification used was 600X.

CHAPTER V

RESULT AND DISCUSSION

The results of this investigation are divided into five sections, each of which is dependent on the others. First, many samples of different oxide-oxide systems, such as $MgO-UO_2$, $BaO-UO_2$, $SrO-UO_2$, $CaO-UO_2$, $Al_2O_3-UO_2$. were internally melted by induction heating and examined to see what type structure formed. The system $MgO-UO_2$ was selected from the above list for further testing because it yielded the best oxide-oxide eutectic structures. Second, various ratios of MgO and UO_2 were unidirectionally solidified to examine the effect of composition changes on eutectic structures. Third, the influence of growth rate on oxide-oxide structures was studied using the ideal $MgO-UO_2$ mixture established in the second phase of this investigation. Lastly, tungsten was added to the system $MgO-UO_2$ to examine the solidification behavior of a ternary system consisting of two refractory oxides and a refractory metal.

Internal Melting and Solidification Behavior of UO_2 with Various Refractory Oxides

The first investigation determined if the various oxide- oxide systems were suitable for internal melting

Table 3**

Induction Melting Behavior of Binary Oxide-Oxide and Oxide Carbonate at 3.5 mhz

Starting Mixture	Preheating Temp. (^{o}C)	Coupling	Melted	Gas	Comment
1. UO_2 + 11 wt% Al_2O_3	1450	yes	yes	N_2	melted out easily after coupling
2. UO_2 + 25 wt% Al_2O_3	1450	yes	yes	$H_2 + N_2$	same as above
3. UO_2 + 20 wt% $BaCO_3$	1490	yes	yes	N_2	some arcing when lowering
4. UO_2 + 20 wt% $SrCO_3$	1550	yes	yes	N_2	melted out a lot, just the lower part of the pellet was melted
5. UO_2 + 20 wt% $CaCO_3$	1520	yes	yes	N_2	forming a lot of smoke during the whole process
6. UO_2 + 20 wt% CaO	1490	yes	yes	N_2	spilled out a lot
7. UO_2 + 18 wt% MgO	1550	yes	yes	N_2	easily to be coupled and form stable melting zone

** All of the above experiments were grown at a rate near 4.5 cm/ hr.

by induction heating and if ordered structures formed. The test mixtures were composed of UO_2 and one of the following compounds: MgO, BaO, SrO, CaO, Al_2O_3.

A compilation of the test results including preheating temperatures, rf coupling information, melting behavior and various comments for all the above materials are presented in Table 3.

In every respect the UO_2-MgO system was found to be the best regarding its internal induction melting behavior and the resultant oxide-oxide eutectic structures. A detailed description of the solidification characteristics of this system is presented in the next section.

It was possible to inductively melt UO_2 with the alkaline earth oxides, CaO, BaO and SrO (using the carbonates as starting materials) and achieve areas of ordered growth. Figures 12, 13, 14 and 15 show longitudinal pictures of these systems. The UO_2-CaO mixtures showed extreme vaporization during growth, especially when $CaCO_3$ was used with the UO_2. The evolation of CO_2 may have provided oxygen leading to the formation of a volatile uranium oxide phase. The UO_2- CaO pellets hydrated very rapidly in air which slowly destroyed the samples. Polishing the samples containing CaO was practically impossible using water because of the hydration reaction. Consequently, structures in this system could not be observed.

The system UO_2-BaO formed two types of structures during solidification. Most of the melted area revealed an unordered coarse intergrowth of the two phases (Figure 12), near the edges of the molten zone, a layer of ordered UO_2-BaO eutectic structure (Figure 13) was typically found adjacent to the skin of the sample. It should be noted that it was difficult to find a $BaCO_3$ powder which 'pressed well' to form a UO_2-$BaCO_3$ pellet suitable for induction melting.

The UO_2-SrO mixture were easily melted using induction heating and an ordered array of SrO rods about 4 microns in diameter were uniformly dispersed in the UO_2 matrix (Figure 14).

Several attempts were made to solidify UO_2- Al_2O_3 mixtures using the internal melting technique but much care was needed because the molten interior of the pellet easily spilled through the thin sample skin. Arcing was also a serious problem with this system. Figure 15 shows the structure of the UO_2- 11 w/o Al_2O_3 mixture consisting of spherical shaped primary UO_2 particles surrounded by a very fine UO_2-Al_2O_3 eutectic structure. This microstructure indicates the eutectic composition in the UO_2-Al_2O_3 system contains greater than 10 w/o Al_2O_3.

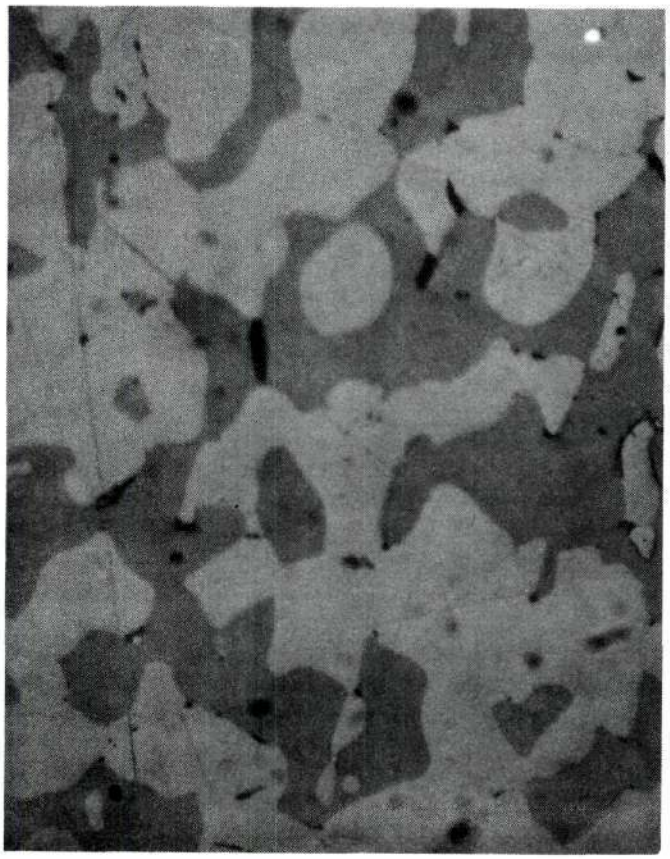

Figure 12. Longitudinal Section of UO_2-20 w/o $BaCO_3$. Most of the Melted Area Revealed and Unordered Coarse Intergrowth of the Two Phases (Light Field 600X).

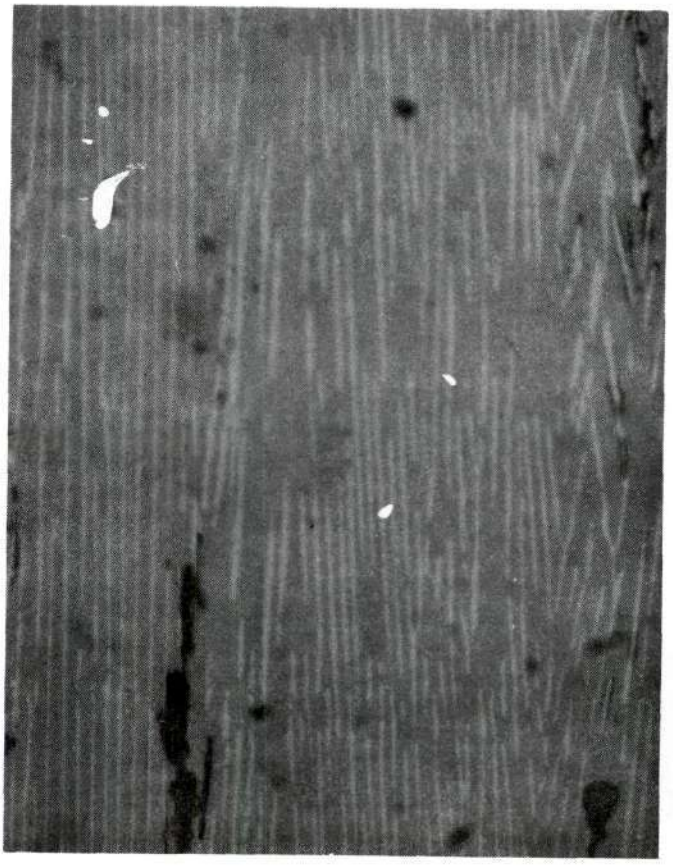

Figure 13. Longitudinal Section of UO_2-20 w/o $BaCO_3$. Eutectic Structure Was Typically Found Adjacent to the Skin of the Sample (Light Field 600X).

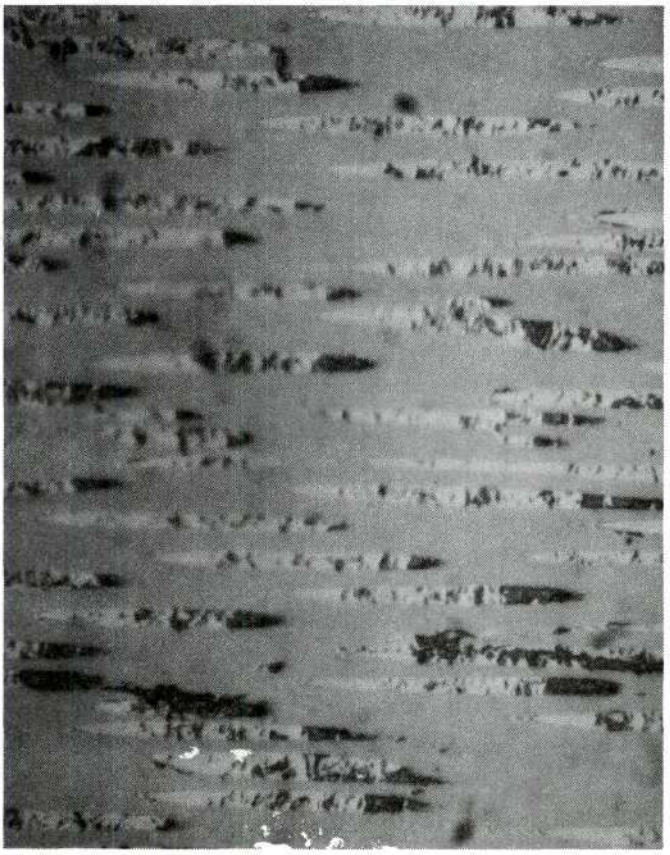

Figure 14. Longitudinal Section of UO_2- 20 w/o $SrCO_3$. SrO Appeared as Rods About 4 Microns in Diameter in the Matrix of UO_2 (Light Field 600X).

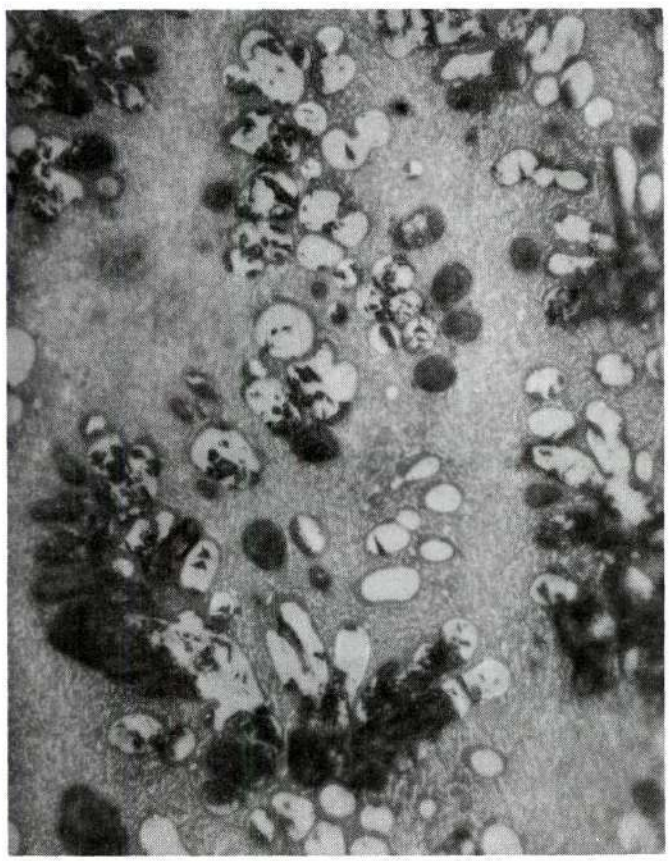

Figure 15. Longitudinal Section of UO_2- 10 w/o Al_2O_3. Spherical Shaped Primary UO_2 Particles Surrounded by a Very Fine UO_2-Al_2O_3 Eutectic Structure (Light Field 600X).

Determination of the Optimum UO_2-MgO Ratio to Form Eutectic Structures and Explanation of Some Structure Faults

In the previous section it was shown that MgO-UO_2 could be easily internally melted by induction heating and unidirectionally solidified to form eutectic structures. In this section the experiments designed to find the optimum composition of MgO-UO_2 for eutectic growth are described. The eutectic composition is that combination of components in a simple system having the lowest melting temperature of any ratio of the components and is located at the intersection of the two solubility curves in a binary phase diagram. For the UO_2-MgO system, the eutectic composition is about 50 mole % UO_2 and 50 mole % MgO or 85 w/o UO_2 and 15 w/o MgO (Figure 16)[25].

Based on the phase diagram UO_2-MgO, pellets containing 10, 15, 18, 20, 25 weight % MgO were internally melted and examined for the presence of eutectic structures. Table 4 presents a summary of the results for these runs.

First, a pellet of UO_2 plus 10 w/o of MgO was preheated to a temperature of 1550°C in a dynamic atmosphere of 500 cc/min of N_2. This mixturecoupled easily, was internally melted and the pellet was lowered for 3.5 cm at a rate of 4.5 cm per hour. Examination of the sample, indicated the amount of UO_2 in this mixture was too high because there were areas of primary UO_2 throughout the melt

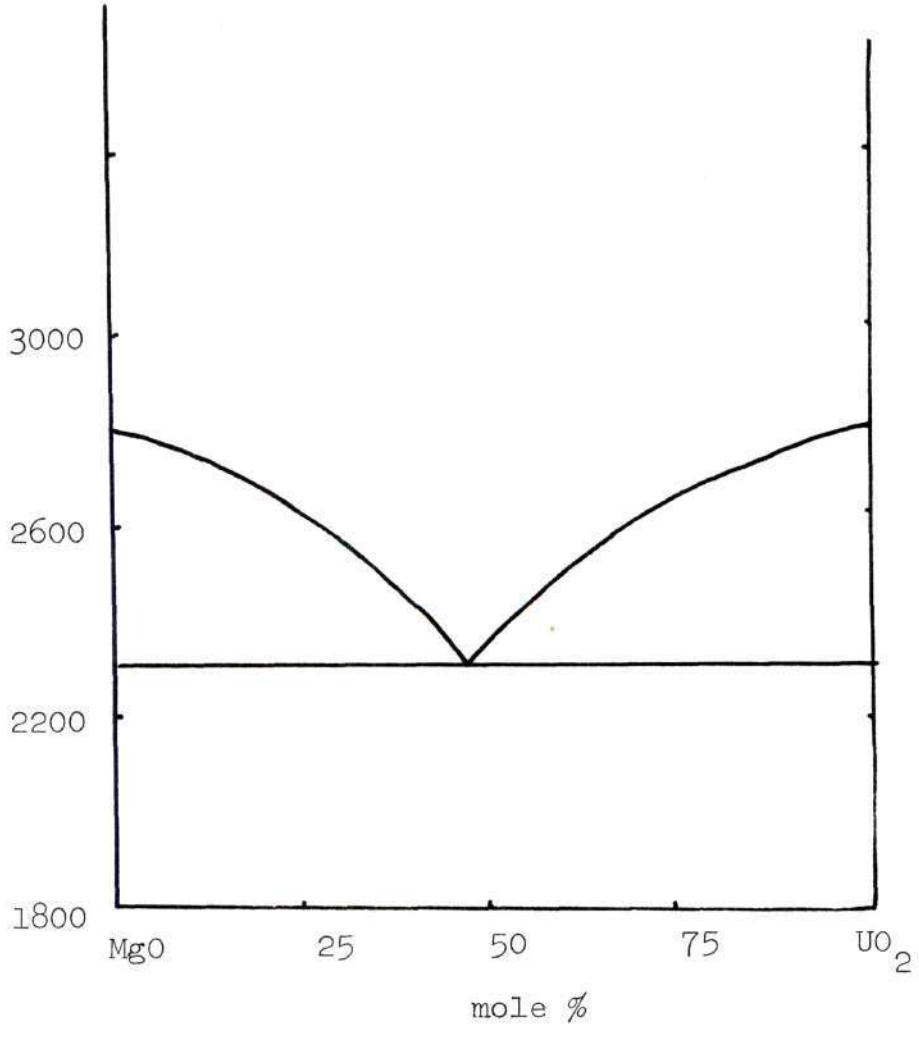

Figure 16. Phase Diagram of $MgO-UO_2$

Table 4

Effect of Varying the MgO Content on the Unidirectional Solidified UO_2-MgO Composites **

w/o MgO in starting mixture	Preheating temp.(°C)	Comments
10%	1550	Extensive areas of primary UO_2 formed.
15%	1530	Uniform eutectics formed.
18%	1540	Uniform eutectics formed.
20%	1540	Uniform eutectics formed.
25%	1550	Some MgO primary phase formed at the edge of the metal.

** All the samples were grown at a rate of approximately 4.5 cm/hr in an N_2 atmosphere, and the power was cut 10% to avoid the spilling of the melt when the pellet had been lowered about 70% of its height and the void was just above the last turn of the coil.

zone. Figure 17 is a longitudinal section of this sample and it shows the round shaped primary UO_2 surrounded by eutectic microstructure. The formation of primary oxide occurs because as the cooling of the uranium dioxide rich melt proceeds, the primary excess phase, UO_2, will solidify at a higher temperature than the eutectic temperature. Therefore the remaining liquid will move down the liquidus line toward the eutectic composition. Since there will be, at some later time, sufficient undercooling to initiate nucleation of the remaining melt, the resulting structure will be area of primary uranium dioxide surrounded by an area of neat eutectic composition.

Since the 10 w/o MgO sample contained excess UO_2, a pellet containing 15 w/o of MgO was internally melted and lowered the same way as the 10 w/o sample. Examination of this sample showed that it formed a uniform eutectic structure in the melted area, the MgO was rather uniformly dispersed in the UO_2 matrix in a shape of rods or lamellae (Figure 18).

In an effort to completely examine samples on both sides of the eutectic composition a pellet containing 25 w/o MgO was melted using the procedure as before. Examination of this sample showed that the central portion of the melt formed a very uniform eutectic structure, Figure 19, but near the edge of the solidified area, MgO was present as random shaped primary phase areas, Figure 20.

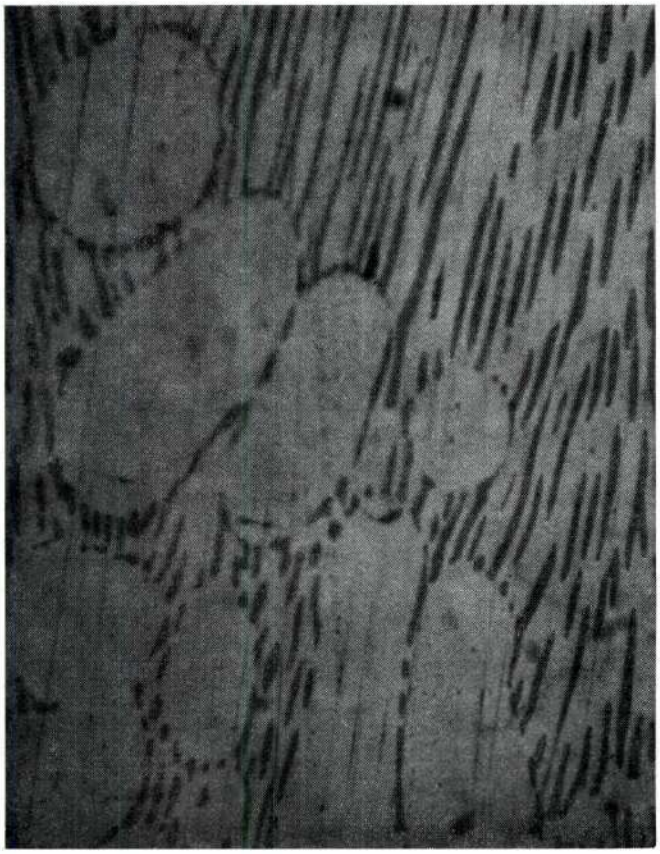

Figure 17. Longitudinal Section of UO_2- 10 w/o MgO. Primary UO_2 Surrounded by Eutectic Microstructure (Dark Field 600 X).

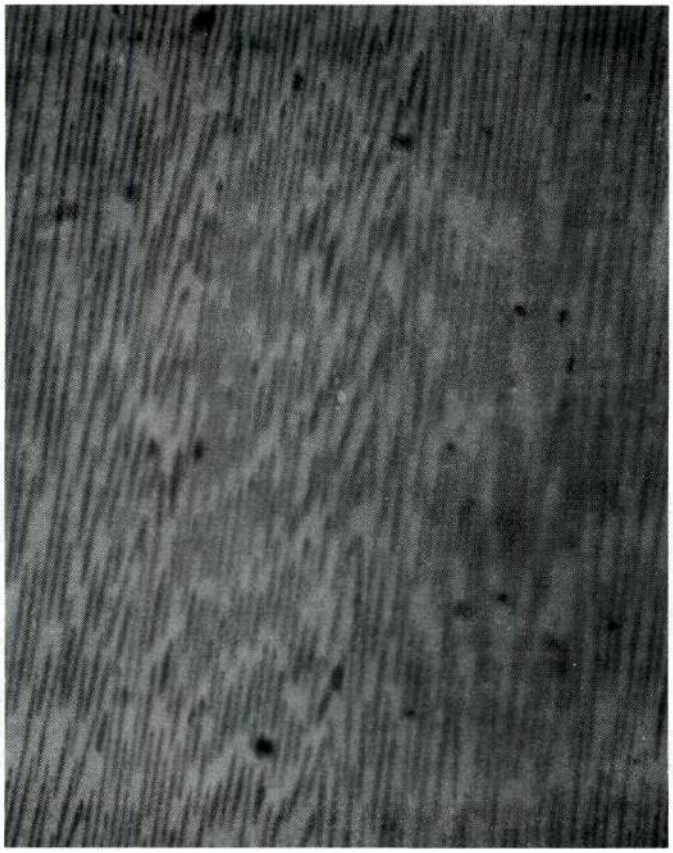

Figure 18. Longitudinal Section of UO_2- 15 w/o MgO.
(Dark Field 600 X).

Figure 19. Longitudinal Section of UO_2- 25 w/o MgO. Central Portion of the Melt Formed a Very Uniform Eutectic Structure (Dark Field 600X).

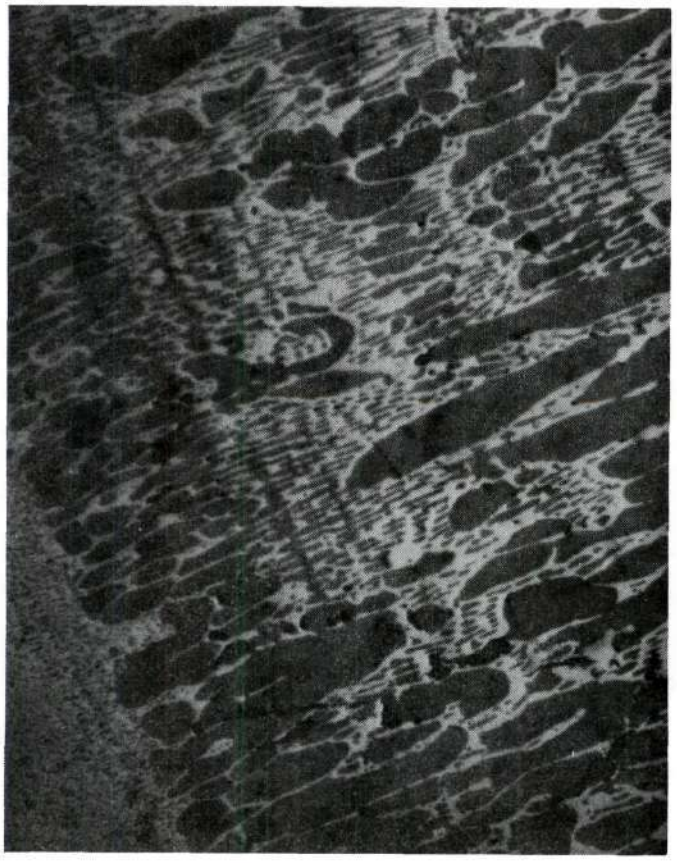

Figure 20. Longitudinal Section of UO_2- 25 w/o MgO. Near the Edge of the Solidified Area MgO Was Present as Random Shaped Primary Phase Areas (Dark Field 600 X).

UO_2-MgO samples containing 18 w/o and 20 w/o MgO were also tested in an attempt to obtain compositions which were free of the primary oxide phases. Both samples formed good eutectic structures in the melted area and the amount of random shaped primary MgO was decreased (Figure 21). Based on these experiments it appears that uniform eutectic structures can be solidified from the UO_2-MgO system for starting mixtures containing between 15-20 w/o MgO. This confirms the phase diagram which indicated the eutectic to be at 15 w/o MgO.

Some of the structural defects observed in samples of the UO_2-MgO were: (a) cells, (b) faults and (c) broken lamellae and rods. Figure 22 shows the cell structure in the UO_2-MgO eutectic and indicates the transformation of a eutectic liquid to a solid is a dynamic process and many complications enter into the picture during the change from the liquid to solid state. As freezing advances in a liquid containing a substance in solution, atoms of the soluble substance are rejected from the solid phase and pile up in front of the advancing interface between the solid and liquid.As a result , under certain conditions a layer of liquid at the interface becomes supercooled. Any prejections from the solid surface get into this supercooled region and then tend to grow rapidly and give the interface a corrugated, cellar form.

Some fault structures were found in lamellar

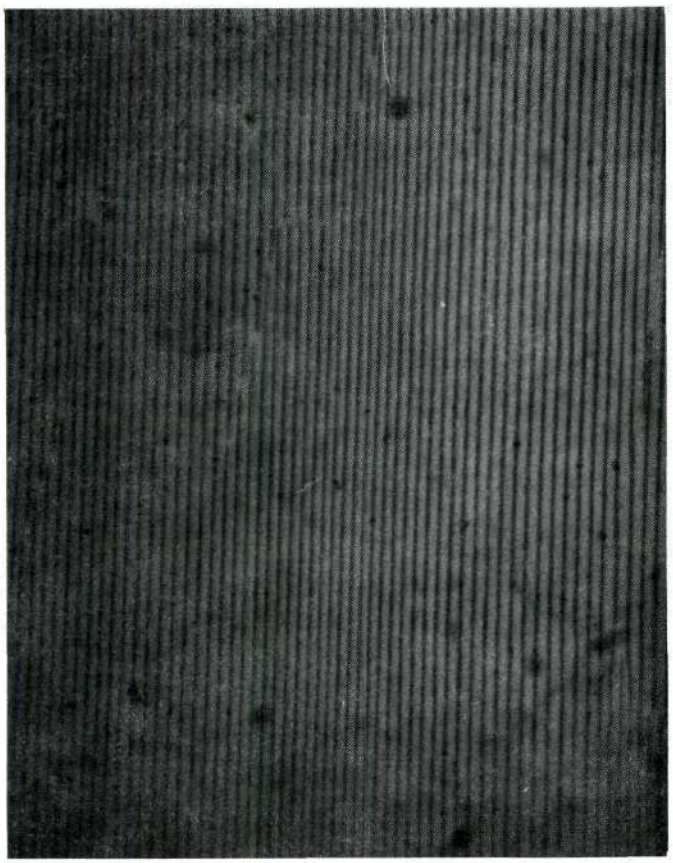

Figure 21. Longitudinal Section of UO_2- 20 w/o MgO.
(Dark Field 600X).

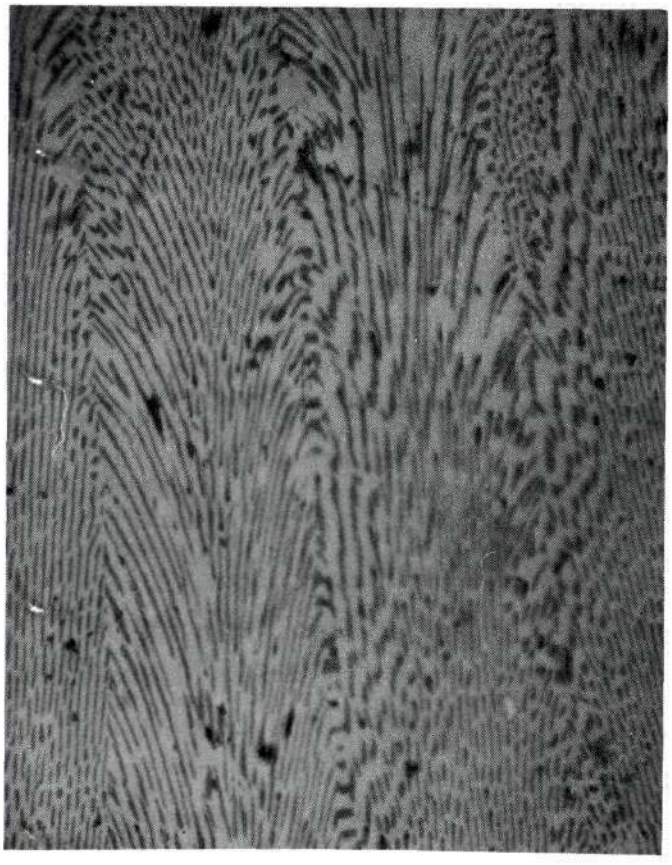

Figure 22. Longitudinal Section of UO_2- 18 w/o MgO.
Cell Structure (Dark Field 600X).

eutectics. They are shown in Figure 23-25. Examing the lamellar structure in the UO_2-MgO system, it was found that the lamellae were sometimes not continuous. On further examination, it was seen that the lamellae on either side of such discontinuity were shifted slightly With respect to each other. These discontinuities are known as fault lines. A count of the number of lamellae on either side of a fault line reveals that in most cases, there is an extra lamellae on one side of the fault line. This is seen in Figure 23 in the circles area, where on one side of the fault line there are eight lamellae and the other side with seven lamellae. This extra line is called a fault. The reason for the formation of faults in lamellae structures is still not very clear, but the occurance of faults during the steady-state lamellar growth is thought to be associated with a changing solid-solid interphase boundary energy during solidification rather than with the maintenance of the steady -state interlamellar spacing. The central part of Figure 24 shows two lamellae structures, one is near fault free and the other is faulted. The faulted lamellae interlamellae spacing is larger than the near faulted-free lamellae. The fact that fault-free lamellae have a smaller interlamellae spacings than the faulted ones formed at the same growth rate may be associated with a lower solid-solid interphase boundary energy. A lower interphase boundary energy permits the formation of more

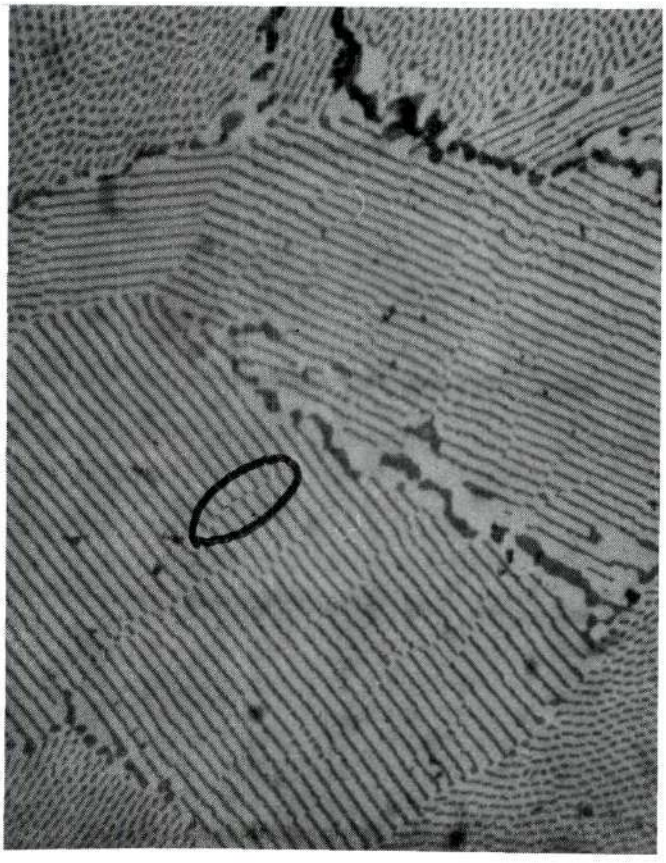

Figure 23. Transverse Section of UO_2- 18 w/o MgO. The Circled Area Shows a Fault Line. One Side Has Eight Lamellar Lines and the Other Side Has Only Seven Lines. (Dark Field 600X).

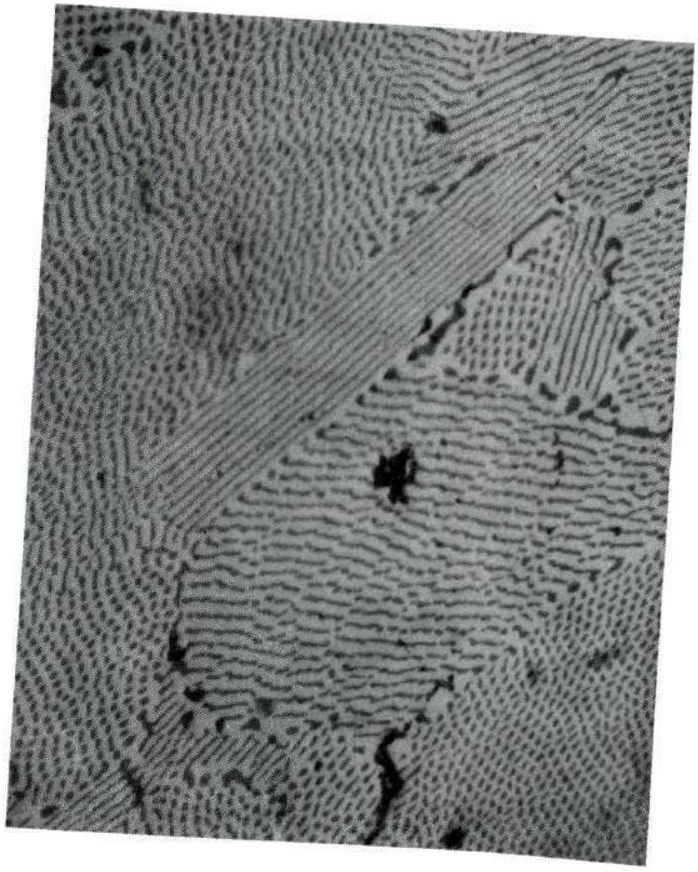

Figure 24. Transverse Section of UO_2- 18 w/o MgO. In the Central Part, There Are Two Regions of Lamellae, One Is Nearly Fault Free and the Other One Is Faulted. The Spacing of the Former One Is Smaller Than the Latter One (Light Field 600X).

boundaries in the solid and hence a smaller interlamellar spacing. It is likely that a lamellar structure can exist over a small range of solid-solid interphase boundary configurations has the lowest energy and occurs in fault free structures. Lamellae having higher interphase boundary energy may attempt to reach the lowest energy as growth proceeds. If different regions of eutectic approach this lowest energy boundary configuration at different rates, they will have different interphase boundary energies and will require different interlamellar spacings. Consequently a range of fault structures will be formed. Figures 23, 24 and 25 show eutectic structures with an increasing fault density; in Figure 25 the structure is further disordered by the presence of broken lamellae and rods. Certainly, there are other possible explanations for conditions leading to faults. Among them is the possibility of a non-uniform lowering rate or rapid but small changes in lowering rate. Also, power fluctuations would change solidification rates producing the same effect.

Effect of Growth Rate on the UO_2-MgO Eutectic Structures.

From the previous stage of this study, an optimum composition of 15-20 w/o MgO in UO_2-MgO was established for forming good eutectic structures. Two pellets, containing 18 w/o MgO and 82 w/o UO_2 were unidirectionally solidified to investigate the effect of growth rate on lamellar (or

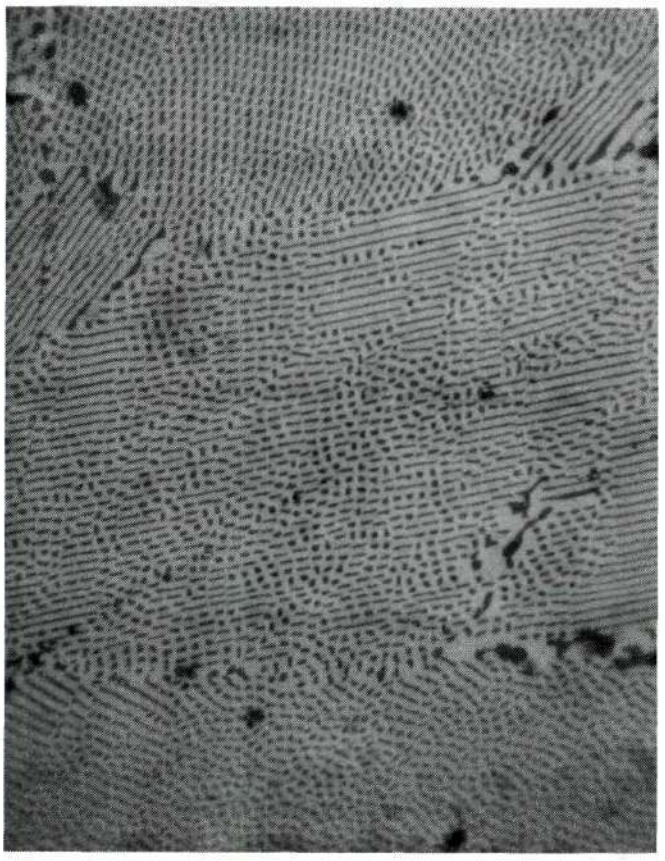

Figure 25. Transverse Section of UO_2- 18 w/o MgO. In the Central Area, There Are Many Broken Lamellae and Rods Caused by Very High Interphase Boundary Energy (Light Field 600 X).

rod -like) size, spacing , and density. The results of these experiments are listed in Table 5.

A general idea about the effect of the growth rate for a given temperature gradient and composition on the lamellar spacing was presented in the literature survey. Basically lamellar spacing increases as the growth rate decreases. Comparing Figure 26 (slower growth rate) with Figure 27 (faster growth rate), the expected change in lamellar spacing is evident.

The lamellae (or rod) density is expected to increase when the growth rate increases, and the diameter of the rods and the width of the lamellae should decrease as the growth rate increases. Figures 28 and 29 are transverse sections of the samples grown at the two growth rates and again the resultant structures are in accord with the theoretical prediction. The results of the experiments are not quite in accord with $\lambda^2 R =$ constant, where λ is lamellar spacing, R is the growth rate; it might be caused by the non-uniform lowering rate during operation.

The Effect of the Addition of Tungsten Into UO_2-MgO System

Since the discovery of metal fiber growth in the oxide-metal composites, much interest has been generated in these composites for electrical applications. This interest is based on the fact that there are millions of less than one micron diameter conducting metallic rods in

Table 5 The Effect of Growth Rate On Eutectic Structure in the $MgO-UO_2$ System

Figure Numbers	Growth Rate	Rod Diameter	Lamellar Spacing	Rod Density per cm^2	Comparative Cell Size
26 & 28	5.0 cm/ hr	1.7 micron	28 micron	18600	small
27 & 29	9.0 cm/ hr	1.0 micron	18 micron	37200	large

** The composition of the $MgO-UO_2$ samples were 18 w/o MgO and 82 w/o UO_2

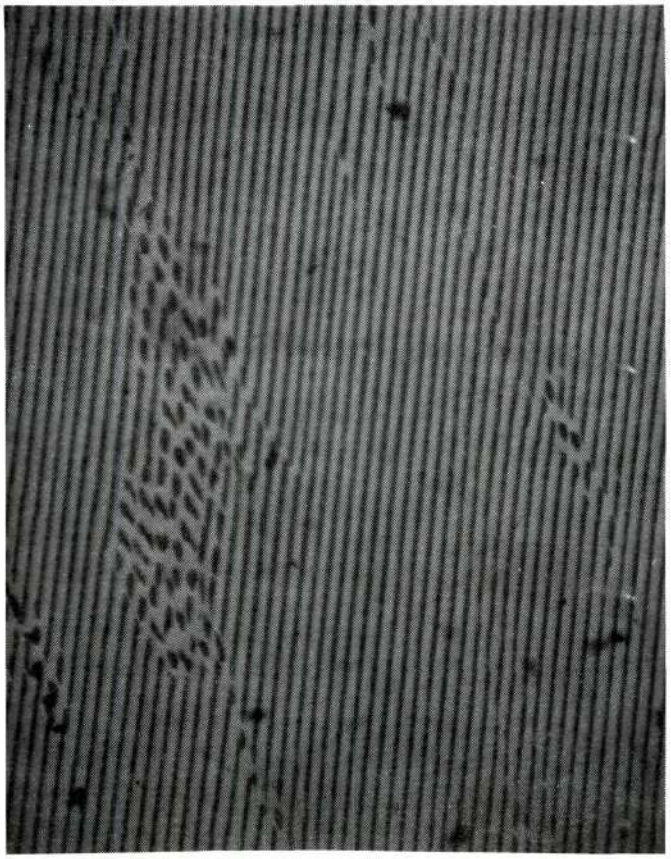

Figure 26. Longitudinal Section of UO_2- 18 w/o MgO.
Lamellar Spacing 28 Microns, Growth Rate 5.0 cm/hr.
(Light Field 600X).

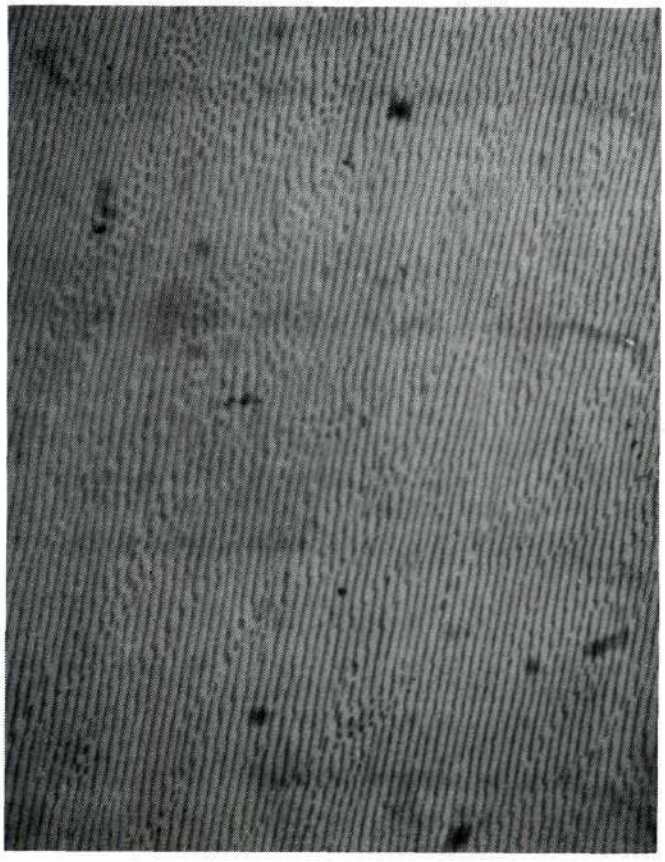

Figure 27. Longitudinal Section of UO_2- 18 w/o MgO. Lamellar Spacing 18 Microns, Growth Rate 9.0 cm/hr. (Light Field 600 X).

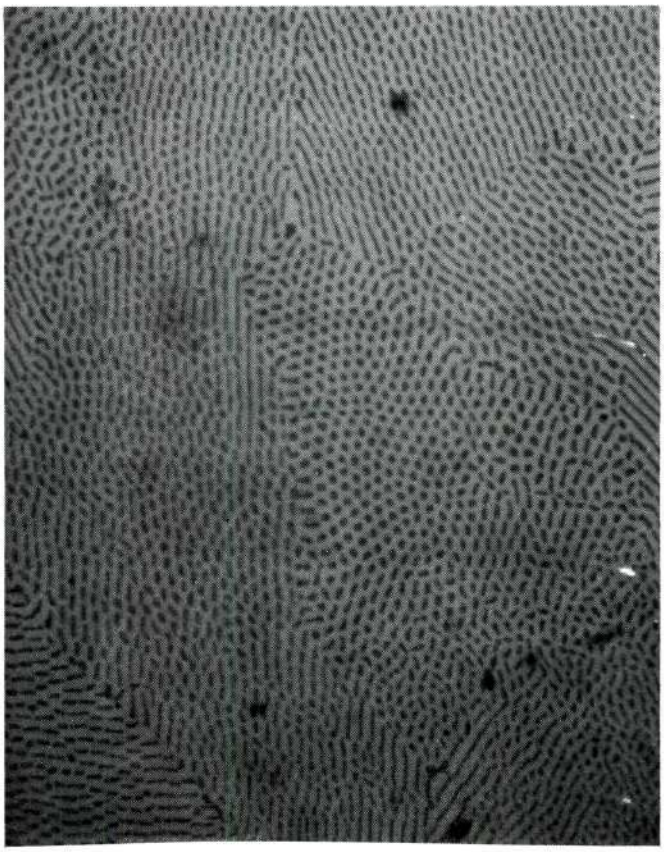

Figure 28. Transverse Section of UO_2- 18 w/o MgO.
Rod Density 18600 Rods/cm^2 . Rod Diameter
1.7 Microns. Growth Rate 5.0 cm/hr.
(Light Field 600 X).

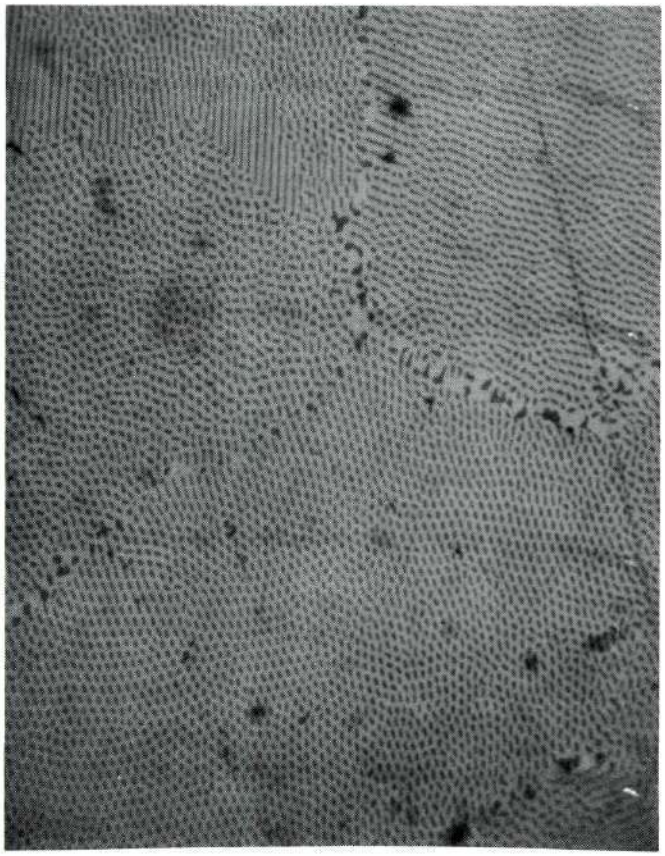

Figure 29. Transverse Section of UO_2- 18 w/o MgO. Rod Density 37200 Rods/cm^2 . Rod Diameter 1.0 Microns. Growth Rate 9.0 cm/ hr. (Light Field 600X).

a square centimeter of an insulating matrix. This geometry is ideally suited for use in microcircuits and electron emission.

Since mixtures of UO_2-MgO formed the best eutectic growth in the systems examined in this study, tungsten was added to different UO_2/MgO ratios to investigave the solidification behavior in the ternary system UO_2-MgO-W.

A compilation of test results including preheating temperature , melting behavior and various comments of those runs are listed in Table 6.

First a pellet of 80w/o UO_2, 10 w/o MgO and 10 w/o W was heated to a temperature of 1500°C in a dynamic atmosphere of 500 cc/min N_2. This mixture coupled easily and was internally melted. Examination of the sample, Figure 30 and 31, showed the W was dispersed in the solidified area as discontinuous fibers and there were extensive areas of primary UO_2. This structure indicated the amount of UO_2 was too high.

Since the previous sample contained excess UO_2, a pellet containing 75 w/o UO_2, 15 w/o MgO and 10 w/o W was internally melted. Examination of the sample showed the amount of UO_2 primary phase had diminished and again the W was dispersed in the composite as discontinuous fibers. (Figure 32).

In an effort to improve the continunity of the W fibers a pellet of 65 w/o UO_2, 15 w/o MgO and 20 w/o W

Table 6 Eutectic Growth Experiments Performed In the Ternary System

UO_2-MgO-W

Mixture (w/o) UO_2/MgO/W	Preheating Temperature	Internal Melting	Atmosphere	Growth Rate	Comments
80/10/10	1500	yes	N_2	5 cm/hr	1,2,3.
75/15/10	1500	yes	N_2	4.7cm/hr	1,2,4.
65/15/20	1500	yes	N_2	4.4cm/hr	1,2,4,5
63/22/15	1500	NO	N_2+H_2		6.

Comments: 1. Arcing a lot if preheated over 1500°C.

2. W randomly dispersed in the solidified area as discontinuous fibers.

3. A lot of UO_2 primary phases.

4. UO_2 primary phases diminished.

5. Some W expelled at the bottom of the melt.

6. Major spill of the molten zone.

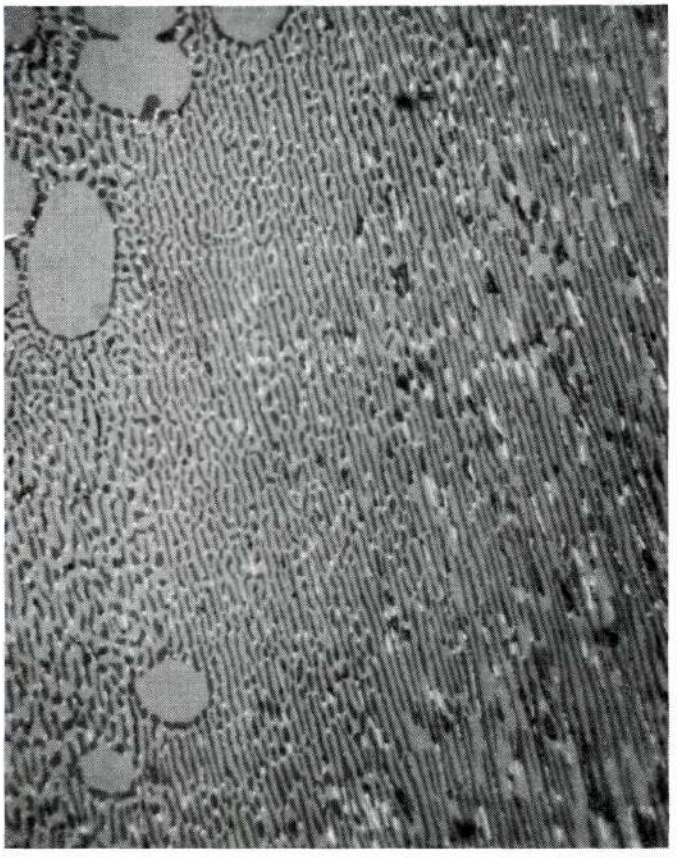

Figure 30. Longitudinal Section of UO_2-80 w/o,MgO-10 w/o , W- 10 w/o (Light Field 600X).

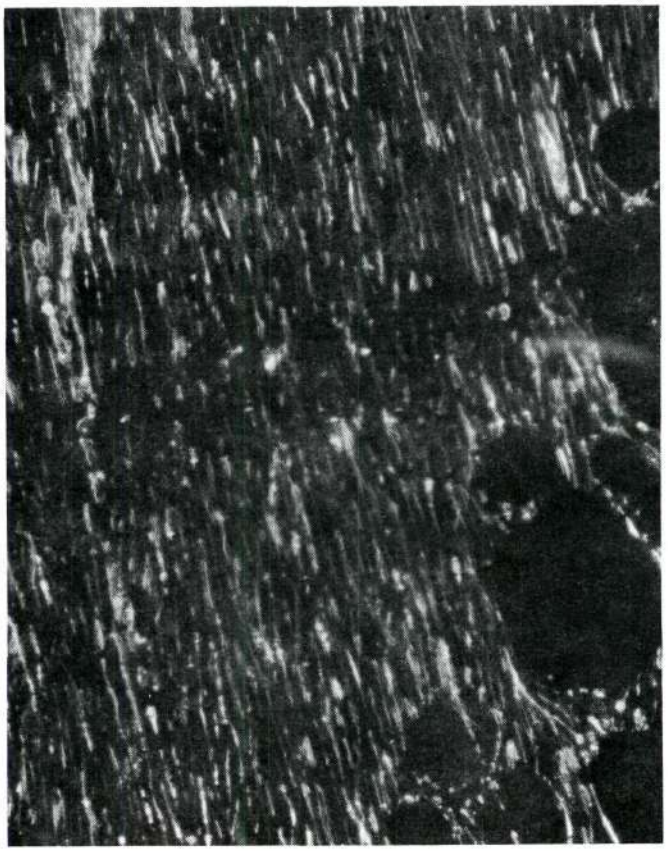

Figure 31. Longitudinal Section of 80 w/o UO_2, 10 w/o MgO, 10 w/o W (Dark Field 600 X).

Figure 32. Longitudinal Section of 75 w/o UO_2, 15 w/o MgO, 10 w/o W (Dark Field 600 X).

was internally melted. Examination of the sample revealed the best ternary eutectic structure obtained in this series of experiments. The transverse section, Figure 33, indicates the W is present as fibers which typically are found at the interfacial region between UO_2 and MgO phases.[26] The UO_2 (light phase) is continuous and the MgO (dark phase) appears as irregularily shaped lathe-shaped particles. The length of W fibers (Figure 34) is not obviously improved over the sample containing 10 w/o W (Figure 32) but it is difficult to assess fiber continuity using dark field microscopy because of the second oxide in the ternary eutectic structures.

In most of these experiments rf arcing was a problem and in an effort to retard the vaporization which promoted arcs , a UO_2- MgO-W sample was melted using a N_2-H_2 atmosphere. Unfortunately this change resulted in a major spill of the molten zone at power settings equivalent to those used in the previous runs. A possible cause for this behavior could be a lowering of the ternary eutectic temperature in a H_2 atmosphere; however, additional work would be required to support this speculation.

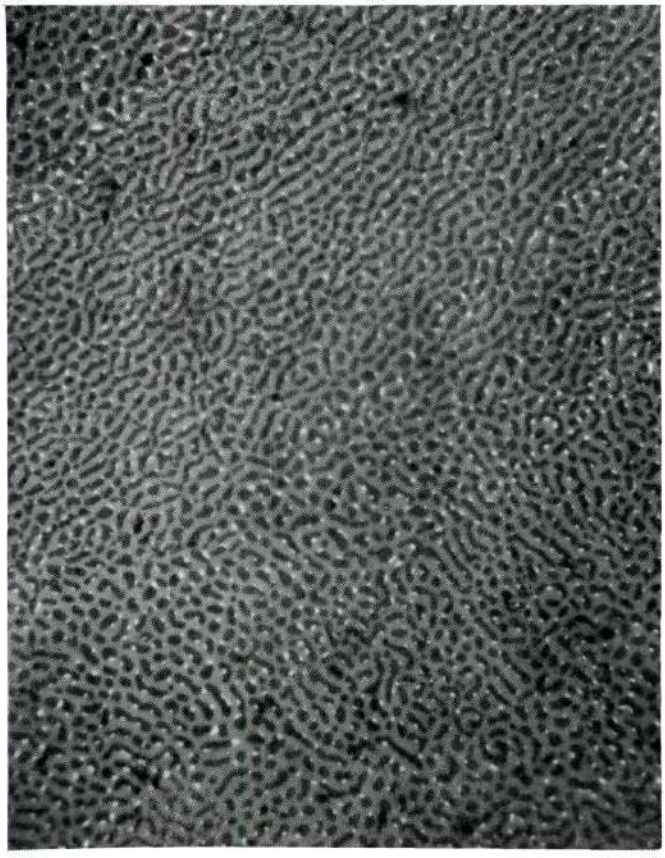

Figure 33. Transverse Section 65 w/o UO_2, 15 w/o MgO, 20 w/o W (Bright Field 600 X).

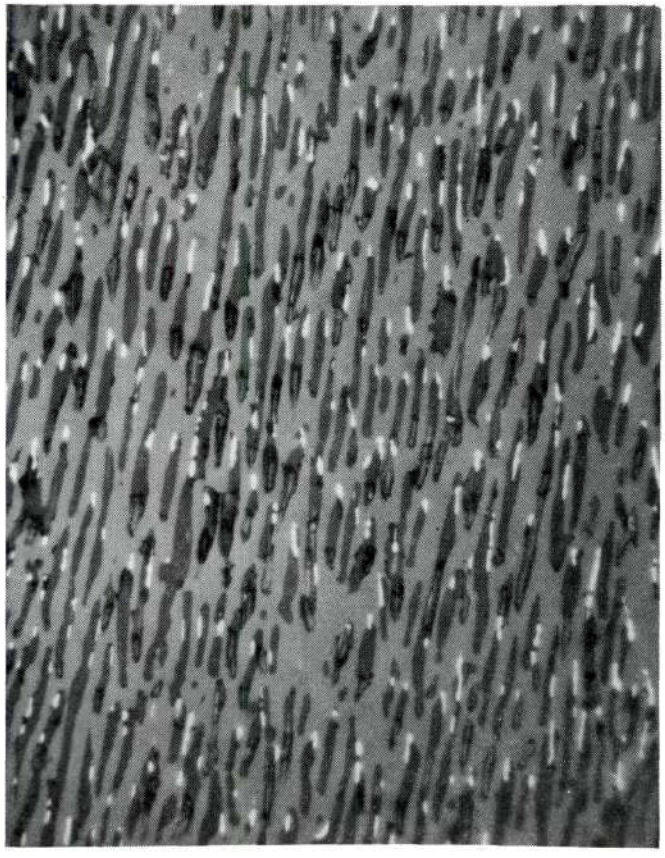

Figure 34. Longitudinal Section of 65 w/o UO_2, 15 w/o MgO, 20 w/o W (Bright Field 600 X).

CHAPTER VI

CONCLUSIONS

1. Oxide mixtures of UO_2 with the alkaline earth oxides, CaO, BaO and SrO (using the carbonates as starting materials) were internally melted using induction heating and produced areas of ordered eutectic growth.

2. The system UO_2-MgO provided the best eutectic structures and the eutectic composition was established at approximately 15-20 w/o MgO.

3. In the system UO_2-Al_2O_3 , much care was needed because the molten interior of the pellet easily spilled through the thin sample skin when this mixture was solidified using the internal melting technique . Rf arcing was also a serious problem in this system.

4. The effect of growth rate on lamellar (or rod-like) sizes, spacings and density in the UO_2-MgO system was found in accord with the theoretical calculation for eutectic growth in metal-metal systems.

5. The addition of tungsten to the UO_2-MgO system formed a ternary eutectic consisting of irregular W fibers and MgO rods dispersed in the UO_2 matrix.

BIBLIOGRAPHY

1. Kraft, R. W.,"Controlled Eutectics," Scientific American, Jan. 1967, pp 86.

2. Chadwick, G. A., "Eutectic Alloy Solidification," Progress in Material Science, Vol. 12, 1963, pp. 113

3. Tiller, W. A.," Liquid Metals and Solidification," American Society For Metals. Clevelane, Ohio, 1958.

4. Jackson, K. A. and Hunt, J. D.," Lamellar and Rod Eutectic Growth," Transactions of the Metallurgical Society of AIME, Vol. 236, August, 1966.

5. Mollard, F. R. and Flemings, M. C.," Growth of Composites from the Melt," Office of Naval Research Technical Report, No. 2, Nov. 1966.

6. Chadwick, G. A.," Interlamellar-Spacing Measurements in Certain Binary Eutectic Systems," Institute of Metal Journal, Vol. 92, 1963-64.

7. Li, C. and Weart, H. W.," On Steady State Phase Transformations," J. Metals, 14, 86, 1962.

8. Slakind, M. and Lemkey, K.," Metals with Grow in Whiskers," International Science and Technology. pp. 59-60, March, 1967.

9. Hunt, J. D. and Jackson, K. A., " Binary Eutectic Solidification," Transactions of the Metallurgical Society of AIME, Vol. 236, 1966.

10. Chapman, A. T., et al., " Metal-Grown Oxide-Metal Composites," Semiannual Technical Report, No. 3, Jan. 1972, Advanced Research Projects Agency, DOD, ARPA order No. 1637, Contract No. DAAHOI-71-C-1046, pp.35.

11. Chapman, A. T., et al.," Melt-Grown Oxide-Metal Composites," Final Technical Report No.2, July, 1971, Advanced Research Projects Agency, Department of Defence ARPA Order No. 1637, Contract No. DAAHOI-70-1157, pp23.

12. Chapman, A. T., Gerdes, R. J., Wilson, J. C. and Clark, G. W.," Unidirectional Solidification Behavior in Refractory Oxide-Metal System,"J. of Crystal Growth, 13,14, p. 765-771, 1972.

13. Jen, C. C., " Factors Determining the Eutectic Unidirectional Solidification Behavior of the System UO_2-Ta. UO_2-Nb, UO_2-Mo," A thesis for M. S. in Ceramic Engineering, Georgia Institute of Technology, Sept. 1972.

14. Grykewich, N. E. Jr.," Factors Determining the Unidirectional Solidification Behavior of the System UO_2-W," A thesis for M. S. Degree in Ceramic Engineering, Georgia Institute of Technology, Sept. 1972.

15. Johnson, M. T.," Controlled Eutectic Solidification in the Al_2O_3-$Y_3Al_5O_{12}$ System," A thesis for B.S. degree in Ceramic Engineering, Georgia Institute of Technology, June, 1970.

16. Hulse, C. O. and Batt, J.A.," Preparation and Properties of Directionally Solidified ZrO_2-Y_2O_3 Eutectic," National Materials Advisory Board Report NMAB, 308-I, 129-140, Jan. 1973.

17. Galasso, F. S.,Darby, W. L., Douglas, F. C. and Batt, J. A.," Unidirectional Solidification of the $BaFe_{12}O_{19}$-$BaFe_2O_4$ Eutectic," J. of the American Ceramic Society, pp.333, June, 1967.

18. Viechnicki, D. and Schmid, F.," Eutectic Solidification in the System $Al_2O_3/Y_3Al_5O_{12}$," J. of Materials Science, 4, 84-88, 1969.

19. Venable, D. and Kinn, T. P.," Radio Frequency Heating," in Industrial Electronics Refrence Book, Edited by Electronics Engineers of Westunghouse Electronic Corp., John Wiley and Sons, Inc., p. 348, 1948.

20. Leatherman ,A. F. and Stutz, D. E.," Induction Heating Advances Application to 5800°F," Office of Technology Utilization, National Aeronautics and Space Administration Washington, D. C., 1968.

21. Tudbury, C. A.," Basis of Induction Heating," Vol. 1, John F. Ryder Publisher, Inc., 1960.

22. Warren, R. W.," Floating Zone Growth of Single-Crystal Alakli Halides," The review of Scientific Instruments, 33, p. 1378-80, 1962.

23. Winegard, W. C.," An Introduction to the Solidification of Metals," Institute of Metals, London, 1964.

24. Shewmon, P. G.," Transformations in Metals," Mcgraw-Hill Series in Materials Science and Engineering, N. Y., Mcgraw-Hill, XII, 394 p. 23 cm., 1969.

25. Levin, E. M., Robbins, C. R. and Mcmurdie, H. F., " Phase Diagram for Ceramists," p. 65, 1964.

26. Chalmers, B., Principles of Solidification , John Wiley and Sons, Inc., p. 218, 1964.